Insights into characteristics, sources and evolution of submicron aerosols during harvest seasons in Yangtze River Delta (YRD) region, China

Y. J. Zhang[1,2], L. L. Tang[2,1], Z. Wang[1], H. X. Yu[3], Y. L. Sun[4], D. Liu[5], W. Qin[2], F. Canonaco[6], A. S. H. Prévôt[6], H. L. Zhang[7], and H.-C. Zhou[1]

[1]Jiangsu Key Laboratory of Atmospheric Environment Monitoring and Pollution Control, School of Environmental Science and Engineering, Nanjing University of Information Science and Technology, Nanjing 210044, China

[2]Jiangsu Environmental Monitoring Center, Nanjing 210036, China

[3]State Key Laboratory of Pollution Control and Resource Reuse, School of the Environment, Nanjing University, Nanjing 210093, China

[4]State Key Laboratory of Atmospheric Boundary Layer Physics and Atmospheric Chemistry, Institute of Atmospheric Physics, Chinese Academy of Sciences, Beijing 100029, China

[5]Centre for Atmospheric Science, School of Earth, Atmospheric and Environmental Sciences, University of Manchester, Manchester M13 9PL, UK

[6]Laboratory of Atmospheric Chemistry, Paul Scherrer Institute, Villigen PSI 5232, Switzerland

[7]Handix LLC, Boulder, CO 8031, USA

Correspondence to: L. L. Tang (lily3258@163.com)

Abstract

Atmospheric submicron particulate matter (PM_1) is one of the most significant pollution components in China. Despite its current popularity in the studies of aerosol chemistry, the characteristics, sources and evolution of atmospheric PM_1 species are still poorly understood in China, particularly for the two harvest seasons, namely the summer wheat harvest and autumn rice harvest. An Aerodyne Aerosol Chemical Speciation Monitor (ACSM) was deployed for online monitoring of PM_1 components during summer and autumn harvest seasons in urban Nanjing, a megacity in the Yangtze River Delta (YRD) region of China. PM_1 components were shown to be dominated by organic fraction (OA, 39% and 41%) and nitrate (23% and 20%) during the harvest seasons (the summer and autumn harvest). Positive matrix factorization (PMF) analysis of the ACSM OA mass spectra resolved four OA factors: hydrocarbon-like mixed with cooking related OA (HOA + COA), fresh biomass burning OA (BBOA), oxidized biomass burning-influenced OA (OOA-BB), and highly oxidized OA (OOA); in particular the oxidized BBOA dominates ~80% of the total BBOA loadings. Both fresh and oxidized BBOA exhibited apparent diurnal cycles with peak concentration at night, when the high ambient relative humidity and low temperature facilitated the formation of semi-volatile organic species. The fresh BBOA concentrations for the harvests are estimated as BBOA = 15.1 × (*m/z* 60 – 0.26% × OA), *m/z* 60 as a marker for levoglucosan-like species. The OA mass decreases with the aging of BB plumes, indicating that the fresh BB plumes contribute to the OA burden significantly. Analysis of air masses back-trajectory indicates that the high BB pollutants are linked to the air masses from the western (summer harvest) and southern (autumn harvest) areas.

1 Introduction

Particulate matter (PM) that is suspended in the atmosphere as atmospheric aerosol plays a

crucial role in regional and global climate system (Ramanathan et al., 2001; Kaufman et al., 2002), air pollution (Sun et al., 2013), ambient visibility reduction (Watson, 2002) and human health (Ge et al., 2011). Significant amounts of PM can be generated from human activities. In particular, biomass burning (BB) activities, e.g., forest fires, wildfire, and agricultural fires, can become the main sources of fine particulate matter ($PM_{2.5}$, particulates $\leq$ 2.5 μm in aerodynamic diameter) and/or submicron particulate matter (PM_1, particulates $\leq$ 1 μm in aerodynamic diameter) (Andreae and Merlet, 2001, Aiken et al., 2010; DeCarlo et al., 2010; Lee et al., 2010; Cubison et al., 2011; Reche et al., 2012; Bougiatioti et al., 2014). Agricultural residues burning is one of the most serious sources leading to severe air quality problems during harvest seasons in China (Li et al., 2007; Wang et al., 2009a; Du et al., 2011; Cheng et al., 2013; Ding et al., 2013). Moreover, China is an agricultural country which has 1.8 billion cultivated fields with a large number of agricultural crop residue (Zhang et al., 2008). Recently, the use of agricultural residues as fuel in China declined. During harvest seasons, farmers usually harvest the crop in the daytime and burn agricultural residues in their fields in the nighttime directly, which may result in BB emission. The understanding of the compositions, sources and processes of atmospheric aerosol particles during harvest seasons is urgently needed to design measures to improve the quality of air in China.

Organic aerosol (OA) composes a large fraction of atmospheric aerosol particles (Zhang et al., 2007). Combination of positive matrix factorization (PMF, Paatero, 1997) and a PMF Evaluation Toolkit (PET, Ulbrich et al., 2009) has been well used to identify and apportion the sources of OA in recent studies (e.g. Lanz et al., 2007; Ulbrich et al., 2009; Allan et al., 2010; Zhang et al., 2005a, 2011; Crippa et al., 2013, 2014; Sun et al., 2013). In addition, an IGOR-based Source Finder (SoFi, Canonaco et al., 2013) with a multilinear engine algorithm (ME-2, Paatero, 1999) can also resolve the emission sources of OA. The current PMF and ME-2 method can only be employed to analyze OA datasets a posteriori (Sun et al., 2012;

Zhang et al., 2011; Canonaco et al., 2013), but cannot be easily utilized in the real-time online estimation of atmospheric OA sources. To identify the sources of atmospheric OA online, an algorithm based solely on organic mass fragments, namely *m/z* 57 (mostly $C_4H_9^+$) and *m/z* 44 (mostly CO_2^+), was developed to estimate hydrocarbon-like OA (HOA) and oxygenated OA (OOA), respectively (Zhang et al., 2005a, 2005b; Ng et al., 2011c). Mohr et al. (2012) also identified cooking OA (COA) in ambient datasets based on the fractions of COA tracers at *m/z* 55 (mostly $C_4H_7^+$) and *m/z* 57 organic mass fragments. Biomass burning organic aerosol (BBOA) is one of the major atmospheric OA species during BB periods (Aiken et al., 2010; Allan et al., 2010). However, limited information is available for estimating the source apportionment of BBOA.

The evolution of atmospheric OA such as oxidation process can significantly influence the ambient concentrations and physicochemical properties of OA (Aiken et al., 2008; Jimenez et al., 2009; Sun et al., 2011b). In the presence of BB source, various volatile and semi-volatile organic precursors can be emitted from the field burning of agricultural wastes, and SOA can be formed from these precursors rapidly (Jimenez et al. 2009; Grieshop et al., 2009; Heringa et al., 2011; Kawamura et al., 2013). What is more, BB plumes can be mixed with urban and regional pollutants during aging processes (DeCarlo et al., 2010; Cubison et al., 2011). In addition to source emissions, the secondary formation, atmospheric transport and diffusion, as well as the mass loadings and oxidation state of ambient OA can be also affected by the aging processes of OA (Jimenez et al., 2009; Cubison et al., 2011; Sun et al., 2011b). Thus, it is important for understanding the nature of atmospheric OA to investigate the evolution of OA and the evolution process effects.

This study investigates the characteristics of PM_1 species using an Aerodyne Aerosol Chemical Speciation Monitor (ACSM), and OA mass spectra are analyzed with PMF model during summer and autumn harvests in the YRD region; the evolution of OA and the effects

of the evolution process on PM burden were also investigated. Combination of back-trajectory analysis and local wind meteorology was used to investigate the source origins.

2 Experimental methods

2.1 Sampling site description

With a population of more than 8 million and an area of ~ 6597 km^2, Nanjing, a megacity, is a representative Chinese city in terms of the pollution characteristics of the YRD region. Local and regional air pollution events frequently occur in Nanjing, mainly caused by emissions of mixed aerosols from fossil fuel burning, residential activities, and agricultural residues burning (Wang et al., 2009a; Ding et al., 2013). In this study, all kinds of data was collected in urban Nanjing (118°46'N, 32°05'E) from June 1 to 15, and October 15 to 30, 2013, corresponding to two harvest seasons in a year, namely the summer wheat harvest and autumn rice harvest. The sampling site was located on the roof of a six-story building approximately 18 m above ground level, ~15 m from the nearest heavy-traffic road, and ~50 m from the nearest restaurants and residents. As a matter of fact, there is no agricultural field in the urban Nanjing areas. This means that the urban Nanjing site is significantly influenced by the BB plumes originated the rural areas and undergone the aging in BB plumes measured dozens or hundreds of kilometers away from the fire locations, but is little/negligibly influenced by the local BB. In addition, the local cooking and traffic emissions can also significantly affect the PM pollution in this sampling site. Therefore, in the presence of BB plumes, the mixed/complicated air pollution will occur in urban Nanjing during the harvest seasons.

2.2 Instrumentation and data analysis

2.2.1 Measurements

The ambient non-refractory submicron aerosol (NR-PM_1) species, i.e., OA, nitrate, sulfate, ammonium, chloride, were continuously measured using ACSM from June 1 to 15, and October 15 to 30, 2013. Detailed descriptions of ACSM can be found in previous studies (Ng et al., 2011a; Sun et al., 2012). Briefly, the ambient aerosols were drawn into the room using a ½ inch (outer diameter) stainless steel tube at a flow rate of ~3 L min^{-1}, of which ~84 cc min^{-1} was sub-sampled into the ACSM. Moreover, ACSM was operated at a time resolution of about 15 min with a scan from *m/z* 10 to 150 amu at 500 ms amu^{-1} rate, which corresponds to the settings of Sun et al. (2012).

An online analyzer, Monitoring of Aerosols and Gases (MARGA, model ADI 2080 Applikon Analytical B. V. Corp., the Netherlands), was deployed to measure the mass concentrations of a major water-soluble inorganic ion (potassium ion, K^+) in the aerosols. A $PM_{2.5}$ cyclone inlet was used to remove coarse particles. Ambient air was sampled into a liquid with a flow rate of 16.7 L min^{-1}. The detection limit of K^+ is 0.09 μg m^{-3}. The MET ONE BAM-1020 and the 7-wavelength aethalometer (Magee AE31) were also employed to measure PM_1 and ambient atmospheric BC in $PM_{2.5}$, respectively. CO was measured using an gas analyzer (Thermo Scientific, Model 48i). Ambient meteorological parameters including ambient temperature (*T*), relative humidity (RH), precipitation, wind speed (WS), and wind direction (WD) were obtained from a ground meteorology station located on the same six-story building as the sampling site.

Daily fire locations used in this study were available from MODIS (Moderate-resolution Imaging Spectroradiometer) mounted on NASA's Terra and Aqua satellites, NASA's Earth Observing System (EOS) (https://earthdata.nasa.gov/data/near-real-time-data/firms). MODIS can present fire distributions in details at 1 km resolution through Fire Information for

Resource Management System (FIRMS) on global scale (Justice et al., 2002; Kaufman et al., 2003). As shown in Figure S1 − S2, all agricultural fire locations (red dots) in the YRD region were detected by the remote sensing retrieval of MODIS from June 1 to 15, and October 15 to 30, 2013 (https://firms.modaps.eosdis.nasa.gov/firemap/).

2.2.2 ACSM data analysis

An ACSM Data Analysis Software package, ACSM Local (Ver. 1.5.2.0.0, released April 25, 2012) written in Wavemetrics Igor^{TM}, was used to analyze the ACSM dataset. More details of procedures have been described in the studies of Ng et al. (2011a) and Sun et al. (2012). The ACSM calibration is based on a combination of a Differential Mobility Analyzer (DMA, TSI model 3080) and Condensation Particle Counter (CPC, TSI model 3775) for the ionization efficiency (IE) and relative ionization efficiencies (RIEs). Pure ammonium nitrate (NH_4NO_3) particles (size selected by 300 nm) are used for the quantitative measurements, because NH_4NO_3 vaporizes with 100% efficiency (Ng et al., 2011a). The RIEs values usually used in Aerosol Mass Spectrometer (AMS) ambient concentration calculations (Canagaratna et al., 2007) are the default values of organics (1.4), nitrate (1.1), sulfate (1.2), and chloride (1.3) in this study. Moreover, the RIE value of ammonium is 7.04, and the response factor (RF) value of nitrate is 3.96×10^{-11} in this study. In addition, the mass concentrations of ambient aerosol need to be corrected for particle collection efficiency (CE) (Middlebrook et al., 2011). CE = 0.5 is found to be representative with data uncertainties generally within 20% (Canagaratna et al., 2007; Middlebrook et al., 2011). The CE values observed in previous studies range from 0.43 to 1, due to (a) shape-related collection losses at the vaporizer from inefficient focusing of non-spherical particles, (b) particle losses at the vaporizer because of bouncing of solid particles before they are completely vaporized, and (c) particle losses in the aerodynamic inlet as a function of particle diameter (Allan et al., 2004; Zhang et al., 2005b; Canagaratna et

al. 2007; Middlebrook et al., 2011). In this study, we selected the CE value for OA, nitrate, sulfate, ammonium, and chloride, respectively, according to the equation CE = max (0.45, 0.0833 + 0.9167 × ANMF) (Middlebrook et al., 2011), in which ANMF is the mass fraction of NH_4NO_3 measured by the ACSM.

The PMF method was applied to analyze OA datasets from the ACSM. More details of procedure for the PMF model can be found in previous studies (Ulbrich et al., 2009; Zhang et al., 2005a, 2011). Furthermore, the OA mass spectra data from the ACSM were determined by combining PMF2 executables with the PMF Evaluation Tool (PET) (Ulbrich et al., 2009). Due to large interferences of internal standard of naphthalene at *m/z*'s 127 − 129, the PMF analysis was restricted to *m/z* 120 (Sun et al., 2012, 2013). Based on the OA dataset from the ACSM, the PMF analysis was performed for 1 to 7 factors. A summary of the PMF results is presented in Figure S6 − S15. For the chosen number of factors, fpeaks were varied in steps of 0.1 from −1 to 1 during the summer and autumn harvest. Four OA factors, i.e., hydrocarbon-like mixed with cooking OA (HOA + COA), fresh biomass-burning OA (BBOA), oxidized BB-influenced OA (OOA-BB), and highly oxygenated OA (OOA) were resolved in this study. The HOA + COA was considered as a factor mixing with COA and traffic HOA in the 4-factor solution, while the "HOA + COA" factor splits into factors with very similar time series in the five- to a seven-factor solution. This means that the PMF analysis of the ACSM OA mass spectra is difficult to distinguish the COA from the traffic HOA in this study. Sun et al. (2010) and Sun et al. (2012) also found a similar phenomenon for distinguishing COA from traffic HOA in a Quadrupole AMS (Q-AMS) and an ACSM OA mass spectra using PMF analysis in Beijing. However, the PMF analysis of high resolution OA mass spectra measured by a high-resolution time-of-flight aerosol mass spectrometer (HR-ToF-AMS) was able to distinguish the COA from the traffic HOA and COA (Huang et al., 2010). For the 3-factor solution, BBOA might be mixed with OOA-BB,

while the 4-factor solution (which contained two BB-related BBOA factors, i.e., BBOA and OOA-BB) seemed to be valid (more details can be found in section 3.2). Recent studies also found the highly similar results with PMF analysis of the OA mass spectra in field studies (Crippa et al., 2013; Bougiatioti et al., 2014; Young et al., 2014). The detailed lists of explanation on the reasons for the selection of the 4-factor solution can be found in Table S4 − S5. In addition, the OA source apportionment for the two harvests will be further discussed in section 3.2.

2.2.3 Back-trajectory analysis

Impacts of various source regions on the PM pollution during the harvest seasons have been investigated using the HYbrid Single Particle Lagrangian Integrated Trajectory (HYSPLIT-4) model developed by NOAA/ARL (Draxler and Rolph, 2003). Accordingly, 48 h back-trajectories at 500 m arrival height above ground level were calculated every 2 h starting at China Standard Time (CST) using a Trajectory Statistics (TrajStat) software developed by Wang et al. (2009b). In this study, the 48 h back-trajectories of air masses were used for further analysis.

3 Results and discussion

3.1 Meteorological factors and PM_1 components

3.1.1 Time series of meteorological factors and PM_1 components

Figure 1 shows the time series of NR-PM_1 species and BC in the presence of different meteorological conditions during the harvest seasons in urban Nanjing, i.e., WS, WD, RH, *T*, and precipitation. During the summer harvest, the average values were 70.7 ± 15.3%, 3.7 ± 1.7 m s^{-1}, and 23.4 ± 4.1 ℃ for the ambient RH, WS, and *T*, respectively. In the autumn harvest, the average values were 54.3 ± 13.7 %, 2.6 ± 1.4 m s^{-1}, and 18.1 ± 3.6 ℃ for the

ambient RH, WS, and *T*, respectively. The frequency distribution of hourly averaged wind direction and speed throughout the summer and autumn harvests were shown in Figure S2 (a – b).

As shown in Figure S3, there is a strong correlation between the MET ONE PM_1 measured by MET ONE BAM-1020 and the PM_1 (= NR-PM_1 + BC) mass concentrations (r^2 = 0.88, *slope* = 1.11), indicating that the ambient submicron aerosols consisted mainly of the NR-PM_1 and BC. Note that the mass concentration of BC in the PM_1 may be overestimated due to the fact that the mass concentration of BC was measured by the 7-wavelength aethalometer for $PM_{2.5}$ and the uncertainties in converting measured light absorption coefficients to carbon concentrations. An overestimation was previously suggested by Huang et al. (2011). The average PM_1 mass for the summer harvest is 38.5 μg m^{-3} with hourly average ranging from 3.6 to 270.6 μg m^{-3}, which is similar to that observed in the autumn harvest (42.3 μg m^{-3}) with hourly average ranging 8.1 to 191.5 μg m^{-3}. Indeed, PM_1 consisted of OA (39%), nitrate (23%), ammonium (16%), sulfate (12%), BC (8%), and chloride (1%) during the summer harvest. During the autumn harvest, PM_1 was composed of OA (41%), nitrate (20%), ammonium (14%), sulfate (11%), BC (13%), and chloride (1%). Table 1 presents a comparison of the average composition of PM_1 between the summer harvest and autumn harvest periods. The average bulk composition of PM_1 during the summer harvest shows similar dominance of OA to the PM pollution during the autumn harvest, but lower mass fractions for other species except nitrate. This is also consistent with some previous findings in the presence of BB source emissions (Crippa et al., 2013; Huang et al., 2013; Bougiatioti et al., 2014). Overall, those species also show a similar contribution between the summer and autumn harvest to the PM_1 mass, suggesting that the PM pollution could be affected by similar pollution sources for the two harvests.

As shown in Figure 1, all aerosol species exhibited very dynamic variations in mass concentrations due to the changes of source emissions, meteorology factors (such as RH, *T*, and planetary boundary layer height), photochemical reactions and regional transport (e.g. the BB plumes). For example, the aerosol species dramatically reduced because of the quick removal processes associated with heavy wet scavenging and/or the dilution of the atmosphere (e.g. 6 – 8 June) during the summer harvest. However, the wet scavenging plays a minor role in changing aerosol loadings with little precipitation during the autumn harvest. OA shows a significant dynamic variation in mass concentrations during the harvest seasons (Fig. 1c), likely due to the changes of source emissions (such as cooking, traffic and/or BB emissions). There are three sharp peaks during the summer harvest (case 1) and autumn harvest (case 2 and case 3). The relationships between the PM pollution, meteorology and chemical composition are presented in three case events (Table S1). The case 1, at 21:00 – 22:00 on 10 June, with the highest PM_1 mass (253.1 μg m^{-3}) can be associated with the northwest wind at 2.5 m s^{-1}. Due to long-range transported pollutants from agricultural fires in the summer harvest (Figure S1), the PM pollution should be affected by the BB plumes from the northwest areas around the urban Nanjing. This speculation is consistent with the highest loadings of K^+, BBOA, OOA-BB, chloride, and BC during the summer harvest. Thus, the case 1 was mainly affected by the BB plumes. Apart from the high loadings of BBOA, OOA-BB, BC, and K^+ seen in the case 2 and case 3 periods, HOA + COA also presents high concentrations. This suggests that both local primary sources emission and regional BB plumes dominate the PM pollution during the case 2 and case 3 periods. Therefore, those findings indicate that indeed BB contributes significantly in the area during the specific time period.

3.1.2 Diurnal variations of meteorological factors and PM_1 components

Figure 2 depicts the diurnal variations of the meteorological factors, i.e., RH, *T*, and WS, and PM_1 species (including OA, nitrate, sulfate, ammonium, chloride, and BC). Generally, the diurnal variations of the meteorological parameters and PM_1 species are similar during the summer and autumn harvest. However, the ambient RH and *T* during summer harvest were higher than those during autumn harvest. OA obviously exhibits three peaks occurring between 6:00 – 8:00, 11:00 – 14:00, and 19:00 – 22:00, which is in agreement with the emission behaviors of pollution sources, i.e., traffic, cooking and/or BB emissions (Allan et al., 2010; Huang et al., 2012; Sun et al., 2012; Crippa et al., 2013). More details of the diurnal variations of the OA components will be presented in section 3.2.

Sulfate presents a weaker diurnal variation during both summer and autumn harvest, and shows a similar concentration during the two harvests. This means the non-volatile character of sulfate and its more regional pollution in the YRD region during the summer and autumn harvest. Similar diurnal trend of sulfate was also found by Huang et al. (2012) in the eastern YRD region. Nitrate presents in a higher fraction of the total PM_1 compared with sulfate, yet with lower concentrations in the afternoon and higher concentrations in the evening during the harvests. Similarly, nitrate also shows a similar concentration for the two harvests during the whole day. In addition, chloride shows a similar diurnal cycle with nitrate during the two harvest seasons. This is in accordance with the volatile properties of ammonium nitrate and ammonium chloride dependent on ambient *T* and RH (Lanz et al., 2007; Sun et al., 2011b, 2012). This also reflects that the photochemical production of HNO_3 cannot compensate for the evaporative loss at the relatively high *T* conditions during the two harvests, which is similar to previous results observed by Huang et al. (2012) in the eastern YRD region and Sun et al. (2012) in Beijing. Furthermore, the higher boundary layer may dilute their loadings during the daytime, and then influence their diurnal cycles (Sun et al., 2012). Chloride is

mainly ammonium chloride (NH_4Cl) and/or organic chlorine-containing species (Huffman et al., 2009; Huang et al., 2012; Sun et al., 2012). During the harvest seasons, the evening high values of nitrate and chloride might be affected by the BB emissions and/or formed via gas-phase and aqueous-phase oxidations.

BC shows a classic diurnal variation with higher loadings appearing in early morning and during nighttime, which is consistent with traffic rush hours in early morning (07:00 – 08:00) and during nighttime (20:00 – 21:00). As previous studies, atmospheric BC is strongly associated with combustion emissions (including traffic and BB sources emissions), particular for BB periods (Sandradewi et al., 2008; Liu et al., 2011, 2014; Crippa et al., 2013). Therefore, the reason for the peak values of BC during the nighttime may be also caused by the BB emissions during the harvest seasons, apart from the effect of traffic source on the BC loadings. The lower concentrations of BC in the afternoon can be associated with the dilution effects of higher planetary boundary layer and reduced traffic emissions.

3.2 Organic source apportionment

Four OA factors (i.e. HOA + COA, BBOA, OOA-BB, and OOA) were identified, as illustrated in Figure 3 and Figure 4. The mean mass concentrations of HOA + COA, BBOA, OOA-BB and OOA during the harvest seasons were presented in Table 1. HOA + COA, BBOA, OOA-BB, and OOA accounted on average for 15% (28%), 7% (7%), 29% (33%) and 49% (32%) of the total OA mass concentrations during the summer (autumn) harvest, respectively.

3.2.1 Hydrocarbon-like and cooking-emission related OA (HOA + COA)

The prominent hydrocarbon ion series of $C_nH_{2n+1}^+$ and $C_nH_{2n-1}^+$ (e.g. 27, 29, 41, 43, 55, 57...) obtained from mass spectrum were characterized as the components of HOA (Zhang et al.,

2005a, 2011; Mohr et al. 2009; Allan et al., 2010). As reported in previous studies, *m/z* 57 ($C_3H_5O^+$ and/or $C_4H_9^+$) and *m/z* 55 ($C_3H_3O^+$ and/or $C_4H_7^+$) are commonly considered as tracers for the primary organic emissions of combustion sources in urban areas, including COA and HOA (Zhang et al., 2005a; Ng et al., 2010, 2011b; He et al., 2010; Sun et al., 2012, 2013; Hu et al., 2013). It is found that there is no significant difference in the mass spectrum between the summer harvest and the autumn harvest (Fig. 3a). Compared with traffic-like OA (Liu et al., 2011; Crippa et al., 2013), the mass spectrum obtained in the present study shows a higher *m/z* 55/57 ratio. Previous studies indicated that high *m/z* 55/57 together with a unique diurnal variation can be used as a diagnostics for the presence of COA (Mohr et al., 2009; Allan et al., 2010; Sun et al., 2012). The mass spectrum of HOA in this study is characterized by more abundant ions, i.e., *m/z* 41 (mainly $C_3H_5^+$), *m/z* 55 (mainly $C_4H_7^+$) and *m/z* 57 (Fig. 3a), which is similar to the characteristics of COA mass spectrum measured by He et al. (2010). As shown in Figure 3, the diurnal variation of HOA + COA shows two pronounced peaks corresponding to noon (a weak peak) and evening traffic/cooking activities (a strong peak). Hence, HOA + COA in this study refers to the sum of traffic-related HOA and COA. Similarly, Sun et al. (2010) and Sun et al. (2012) also found that HOA species in urban ambient were influenced by both traffic and cooking-like emissions. In addition, it is seen that the high HOA + COA concentration (> 6 μg m^{-3}) occurred when WD was from southeast during the summer harvest (Fig. S4). During the autumn harvest, the high concentration of HOA + COA was associated with northerly and easterly winds. This result is well consistent with the areas of local cooking and traffic sources emissions around the sampling site.

3.2.2 Fresh biomass burning OA (BBOA)

As shown in Figure 3b, the mass spectrum of BBOA extracted in this study shows a prominent peak of *m/z* 60 (almost all $C_2H_4O_2^+$) which is a well-known tracer ion for BB

emissions (Alfarra et al., 2007; Aiken et al., 2009; Cubison et al., 2011; Huang et al., 2011; Liu et al., 2011). Levoglucosan was shown to contribute to *m/z* 60 and was found in large amounts in urban, suburban, and rural background atmosphere during BB periods (Maenhaut et al., 2012). In addition, the BBOA is also characterized by higher peaks at masses *m/z* 27, 29, 41, 43, 55, 57, 77 and 91 that are indicative of freshly emitted organic aerosol, because fresh *m/z* 43….. *m/z* 57 can be also from BB-related emissions (Aiken et al., 2009; Heringa et al., 2011; Bougiatioti et al., 2014). For example, primary BBOA (P-BBOA) has a significant contribution from a non-oxygenated ion $C_3H_7^+$ at *m/z* 43, but not from an oxygenated ion $C_2H_3O^+$ (*m/z* 43) in smog chamber experiments by Heringa et al. (2011). The BBOA spectrum profiles with the lack of *m/z* 44 signal (CO_2^+) during the summer and autumn harvest show high correlation (r^2 = 0.82 and r^2 = 0.87) with a result in Paris (Crippa et al., 2013). This spectral pattern also shows much similarity to the spectrum of pure BBOA with the fresh burning condition (flaming phase) in a wood stove (Weimer et al., 2008). Moreover, the spectrum of BBOA in this study is qualitatively similar to published BB spectra from the fresh BB smoke in a smog chamber (Grieshop et al., 2009). These findings suggest that this factor can be related to BBOA with low atmospheric oxidants, and thus this factor might be fresh/primary BBOA during the harvests.

Using soluble K^+ as a tracer for BB has also been reported by previous analyses of BB campaign data (Gilardoni et al., 2009; Aiken et al., 2010; Du et al., 2011; Crippa et al., 2013). The time series of BBOA along with K^+ measured by MARGA is shown in Figure 4b. BBOA is strongly correlated with K^+ (r^2 = 0.95 and r^2 = 0.75) during the summer and autumn harvest respectively (Fig. 5a), suggesting that BBOA and K^+ were from the same source. In addition, the diurnal variation of BBOA shows a pronounced peak at the nighttime, which is consistent with the effects of the BB emissions (Fig. 3). This means that BBOA contributes to POA during the nighttime mainly. This finding is also consistent with the habit of the farmers

in the YRD region, namely that they usually harvest wheat or rice in the daytime and burn off straw in the nighttime during the harvest seasons each year. In addition, chloride correlates well with BBOA (r^2 = 0.61 and r^2 = 0.66) and K^+ (r^2 = 0.60 and r^2 = 0.64) during the harvest seasons (Figure S5). This means that chloride was mainly from the BB emissions and might be in the form of KCl during the BB periods.

3.2.3 Oxygenated OA (OOA) and oxidized BB-influenced OA (OOA-BB)

The mass spectrum of both OOA components (Fig. 3d) was characterized by the prominent $C_xH_yO_z^+$ fragments, mainly CO_2^+ (*m/z* 44) which has been denoted previously found in many AMS studies (Zhang et al., 2005a; Lanz et al., 2007; Sun et al., 2010; Crippa et al., 2013). The mass spectra of OOA by the prominent peak of *m/z* 44 (22.9% and 25.5% of the total OOA signal respectively) during the summer and autumn harvest are strongly consistent with more oxidized OOA component determined (r^2 = 0.91 and r^2 = 0.89, Fig. 3d) in BB-period in Paris (Crippa et al., 2013) and OOA components resolved at other urban sites (Lanz et al., 2007; Ulbrich et al., 2009).

As shown in Figure 4d, the time series of OOA is compared with the sulfate mass loadings. A good correlation was observed between time series of OOA and sulfate mass loadings (r^2 = 0.60 and r^2 = 0.46, Fig. 6) during the summer and autumn harvests, respectively. Previous studies performed at various sites also showed that these two species were secondary with low-volatility property in the atmosphere (Zhang et al., 2005a; Lanz et al., 2007; Ulbrich et al., 2009; Sun et al., 2011a; Huang et al., 2012). Overall, the diurnal pattern of OOA shows relatively stable variation throughout the whole day (Fig. 3). OOA often remains at a high concentration across several days until a change of air mass occurs, which shows a regional production (Sun et al., 2012, 2013). This may be a main reason causing the relatively stable variation through the whole day in this study. Nevertheless, OOA shows a

slight increase at around 12:00 – 15:00, suggesting that OOA might be formed by photochemical processing during the daytime in the harvest seasons. OOA also exhibits higher loadings during the nighttime, probably caused by the aging of BB plumes, in which BB emissions will be further oxidized and begin to transition into OOA (Jimenez et al., 2009, DeCarlo et al., 2010). The uniform distribution of its concentrations is almost in association with all kinds of WD during the summer and autumn harvest respectively (Figure S4). This is a good evidence for explaining the regional pollution of OOA in the YRD region during the harvest seasons.

Additionally, an oxygenated factor with the high degree of oxygenation during the summer and autumn harvest (*m/z* 44, 18.2% and 14.5% of the total factor signal respectively) in its mass spectrum has been resolved as oxidized BB-influenced OA (OOA-BB, Fig. 3c). The mass spectra of OOA-BB are characterized by both the oxidized signals (*m/z* 18, 29, 43 and 44) and the typical marker of BB (*m/z* 60) during the summer and autumn harvest, which correlates well with BB-emission related OOA (OOA_2-BBOA) (r^2 = 0.85 and r^2=0.86) during BB periods at an urban site in Paris (Crippa et al., 2013). It is also highly similar to the mass spectrum of the aged BBOA identified by DeCarlo et al. (2010) for airborne measurements during the MILAGRO campaign, and very in agreement with the aged BBOA from a BB experiment in a chamber study by Heringa et al. (2011). In addition, the mass spectrum of OOA-BB shows more oxygenated degree, compared to mass spectrum of fresh/primary BBOA from PMF analysis in the atmosphere and from laboratory open wood burning (Aiken et al., 2009) and from BBOA in this study. Furthermore, the OOA-BB spectrum shows rather similarity to a BBOA spectrum (dominated by oxygenated ions, i.e. *m/z* 18 and *m/z* 44, and with lower fraction of *m/z* 60) observed in a wood stove with the burning condition of smoldering phase (Weimer et al., 2008). This means that burn phase also plays a significant role in the OOA-BB formation, and thus may influence its loadings in the open BB periods.

The OOA-BB spectrum in this study is also very similar to the spectrum of the secondary OA produced from aged biomass smoke in a smog chamber (Grieshop et al., 2009). The results suggest that OOA-BB may contain some aged/secondary BBOA, although it is not precisely known whether this factor is processed OOA from BB or processed primary BBOA mixed with SOA from another source in the atmosphere, as well as the burn phases. OOA-BB presents a pronounced diurnal cycle with the highest concentration in the evening and early morning during the harvests (Fig. 3), which is very consistent with the diurnal variations of BBOA. This means that the SOA formation from open BB is rapid in short timescales with the high RH and low *T* conditions in the nighttime, because volatile and semi-volatile organic precursors can directly emit from field burning and it will be subsequently transformed into SOA via ozonolysis (Kawamura et al., 2013) and NO_3 reactions in the dark. OOA-BB also shows the relatively low loadings in the daytime, due to the dilution effects by enhanced mixing in the planetary boundary layer and the evaporative loss of semi-volatile components.

As shown in Figure 4c, the OOA-BB time series strongly correlates with K^+ and Δ *m/z* 60 (= *m/z* 60 – 0.26% × OA, in which applied metric of background f_{60} = 0.26 % of OA will be discussed in section 3.4) during the summer and autumn harvest, supporting the BB influence. In addition, the sum of BBOA and OOA-BB also shows high correlation with K^+ and Δ *m/z* 60 for the two harvests (Fig. 5a − b). This suggests that OOA-BB represents an atmospheric mixture of BBOA and OOA, which is similar to a recent HR-ToF-AMS study by Crippa et al. (2013). It is interesting that OOA-BB correlates well with nitrate (r^2 = 0.30 and r^2 = 0.54), yet shows lower correlation with sulfate (r^2 = 0.16 and r^2 = 0.30) for the summer and autumn harvest respectively (Fig. 6). Also, the time series of OOA-BB shows a similar trend as chloride during the two harvest seasons (Fig. 4c). This implies an indication of the semi-volatile character of OOA-BB, which is consistent with the results from a recent filed study in the eastern Mediterranean (Bougiatioti et al., 2014) and some laboratory chamber

studies (Lipsky et al., 2006; Robinson et al., 2007; Yee et al., 2013). Particularly, this also means that aged biomass burning OA (OOA-BB) may be significantly mixed with nitrate in the BB plumes. Healy et al. (2013) also found a similar result in Paris using single-particle mass spectrometer (SP-AMS) and HR-ToF-AMS measurements. As shown in Figure S4, for the BB-emissions related OA (including BBOA and OOA-BB), they show a very similar wind rose pattern with high concentration from southeasterly wind during the summer harvest, and from northerly wind during the autumn harvest. This further supports that the production of OOA-BB is related to the BB plumes.

3.3 Effects of Chemical components on PM pollution

Figure 7 presents the average contributions of PM_1 species and OA components during the summer and autumn harvest, respectively. It is also compared with other sites, including megacities (Mexico City, Paris, Beijing, and Shanghai), suburban/remote areas (Crete, Jiaxing, and Pearl River Delata) (Aiken et al., 2009; Crippa et al., 2013; Huang et al., 2012, 2013; Sun et al., 2012; Bougiatioti et al., 2014). Using the relative contribution of the sum of BBOA and OOA-BB to OA, the harvest season was separated into 3 time periods, i.e., low BB (L-BB, 28% and 29%) period, medium BB (M-BB, 49% and 38%) period, and high BB (H-BB, 93% and 50%) period, during the summer and autumn harvest respectively. We also include averages of some meteorological parameters (i.e. RH, *T*, WS, and WD) for the reference, and these averages are shown in Table S2.

As shown in Figure 7, OA is important in PM pollution in the summer and autumn harvest (39% and 41%). Furthermore, the average contribution of BBOA to OA during the summer harvest (7%) is highly consistent with that in the autumn (7%), while BC shows a higher contribution during the autumn harvest (12%) than that in the summer harvest (8%). This is also corresponding to the contribution of HOA + COA, which shows a higher

contribution during the autumn harvest (28%) than that in the summer harvest (15%). The different boundary layer height and primary sources emission influences on primary pollutants (including BC, HOA and COA) may be all potential causes of such seasonal differences. On average, the total oxidized fraction of OA (including OOA and OOA-BB) accounts for more than 60% (78% for summer and 65% for autumn harvest), which indicates that regional OOA plays an important role in PM pollution in urban Nanjing during the harvest seasons. This is also corresponding to some contention discussed in section 3.2.3. As a comparison, OOA-BB shows a higher contribution to OA in H-BB period than in L-BB period. The contribution of OOA-BB to OA is higher than the contribution of BBOA during the harvest seasons, even in the H-BB period. These findings indicate that "aged" BBOA plays a more significant role in PM pollution than BBOA in the BB plumes, particularly in the H-BB period. This is consistent with recent studies (Grieshop et al., 2009; Heringa et al., 2011; Lathem et al., 2013; Yee et al., 2013; Bougiatioti et al., 2014) indicating that the fresh BB emission OA can be rapidly surpassed by SOA formation within a few hours after its emission.

The secondary inorganic aerosols (including sulfate, nitrate, and ammonium) can be seen in lower fraction in the H-BB period than in the L-BB period. However, the mass concentrations of sulfate, nitrate and ammonium are higher in the H-BB period than in the L-BB period (Table S2) respectively. Therefore, these findings indicate that BB contributes more fractions on organics than that on the secondary inorganic aerosols in the transported pollution air masses. It is interesting that the contribution of nitrate to PM_1 is higher than the contribution of sulfate in the H-BB periods during the two harvest seasons. For example, the average contribution of nitrate to PM_1 is ~18% in the H-BB periods, which is almost twice higher than that of sulfate. However, the contribution of nitrate to PM_1 is very similar to the sulfate contribution in the L-BB periods. All of those indicate the BB is a much more

important source of nitrate, compared to sulfate. Similar results have been observed by Crippa et al. (2013), Healy et al. (2013) and Bougiatioti et al. (2014) during open BB periods.

Figure 8 presents the mass fractions of PM_1 species and OA components as a function of total PM_1 mass loadings, as well as the probability density of total PM_1 mass loadings during the summer and autumn harvest respectively. Overall, the total OA components (i.e. HOA + COA, BBOA, OOA-BB and OOA) remained at a relatively stable level across all mass loadings during the two harvest seasons. However, OOA-BB and BBOA show a significant increase as a function of the PM_1 loadings respectively, highlighting the contribution of OOA-BB arising from BB emissions to PM pollution during the harvest seasons. During the summer harvest, the HOA + COA and BC mass fractions display a slight decrease, suggesting that local primary sources play an important in the low PM pollution period. In addition, the nitrate and sulfate contributions show a slight increase and decrease respectively, indicating additional production of nitrate mass during high PM episodes. During the autumn harvest, it also should be pointed out that the OOA mass fraction shows a slight decrease as the increasing of total PM_1 loadings, which indicates that OOA is of significant importance to the low PM pollution while at high pollution OOA-BB is more crucial. However, the contribution of HOA + COA, BC, and the secondary inorganic species to the total PM_1 loadings did not show clear PM-mass loading dependency, which indicates that the high PM pollution during the autumn harvest may be caused by the synergistic effects of all pollutants.

3.4 Estimation of BBOA directly from a tracer (Δ *m/z* 60)

The BBOA mass loadings during the harvest seasons were estimated using a simple method. As described in previous studies, the parameter f_{60}, fraction of *m/z* 60 in total OA, is considered as a marker of fresh/primary BBOA (Alfarra et al., 2007; DeCarlo et al., 2008; Aiken et al., 2009; Cubison et al., 2011). To estimate the real value of the BBOA loadings,

519 the background level of f_{60} (0.26 ± 0.1%) during little/negligible BB-influence periods
520 (non-BB periods) was determined (Fig. 9). Aiken et al. (2009) and Cubison et al. (2011) also
521 obtained a similar background level of f_{60} (0.3 ± 0.06%) for an urban city in Mexico.
522 Therefore, the levoglucosan-like species in ambient BB plumes was estimated by Δ *m/z* 60 (Δ
523 *m/z* 60 = *m/z* 60 – background value of f_{60} × OA). As shown in Figure 5b, the strong
524 correlations (r^2 = 0.95, r^2 = 0.98, and r^2 = 0.97) between the BBOA and Δ *m/z* 60 with the
525 similar slopes, i.e., 16.3 for summer, 14.6 for autumn, and 15.1 for the total harvest seasons,
526 were observed. The OOA-BB mass loadings also show the high correlations with Δ *m/z* 60 (r^2
527 = 0.95 and r^2 = 0.97), but with very different slopes (74.8 and 64.4) during the summer and
528 autumn harvest respectively (Fig. 5b). As discussed above and by some reports (Aiken et al.,
529 2009; DeCarlo et al., 2010; Cubison et al., 2011; Crippa et al., 2013; Bougiatioti et al., 2014),
530 this can be a good evidence to further support the OOA-BB loadings depended on the aging
531 processes of BB pollutants and its mathematically mixing of sources in the BB plumes. Aiken
532 et al. (2009) also found that BBOA strongly correlated with Δ *m/z* 60 mass loadings (r^2 = 0.91,
533 *Slope* = 34) during the BB/wood-smoke periods in Mexico City. Furthermore, Lee et al.
534 (2010) obtained a strong relationship between BBOA and *m/z* 60 mass loadings (r^2 = 0.92,
535 *Slope* = 34.5) through a wildland fuels fire experiment in the lab. Thus, we reconstructed the
536 time series of BBOA to compare the relationship between the extracted BBOA by PMF
537 model (PMF BBOA) and the estimated BBOA. As shown in Figure 10, an excellent
538 agreement is observed between the identified and reconstructed BBOA concentrations during
539 the total harvest seasons (r^2 = 0.97). Therefore, the BBOA component during the BB periods
540 in urban Nanjing of the YRD region can be estimated with the equation of BBOA = 15.1 ×
541 (*m/z* 60 – 0.26% × OA) for the harvest seasons.
542

3.5 Evaluation of OA

To further investigate the probable importance of the aging and/or mixing processes of BB plumes, the total BB-related OA (BBOA + OOA-BB) to ΔCO ratio as a function of the f_{44} during the summer and autumn harvest respectively is shown in Figure 11. The CO background is determined as 14.9 μg m^{-3} for summer harvest and 17.9 μg m^{-3} for autumn harvest, respectively, based on an average of the lowest 5% CO during two plumes (Takegawa et al., 2006). The ratio of BBOA + OOA-BB to ΔCO can remove the effect of dilution in the regional air (DeCarlo et al., 2008). As discussed in de Gouw et al. (2005), Aiken et al. (2008), Jimenez et al. (2009), and Ng et al. (2010), the f_{44} can be considered as indicator of atmospheric aging due to photochemical aging processes leading to the increasing of f_{44} in the atmosphere. Overall, the (BBOA + OOA-BB) / ΔCO ratio shows an obvious reduction with increasing of f_{44} values during the summer and autumn harvest respectively, in the absence of traffic and cooking-like plumes. This is likely due to a synergistic effect of the rapid formation of OOA from BB plumes and the mixing of BBOA with regional OOA and/or CO. Similar results have been found by DeCarlo et al. (2010), from aircraft measurements during MILAGRO in Mexico City and the Central Mexican Plateau. It is interesting that the BB plumes in the summer harvest show a higher oxidation level (Δf_{44} = 0.04, within the two dashed lines of Fig. 11) than that in the autumn harvest (see also Fig. 9). This might be a potential factor leading to a higher oxidation level in the mass spectra of OOA-BB in summer harvest, compared to that in the autumn harvest (Fig. 3c).

Figure 12a depicts the evolution process of OA with the f_{44} vs. f_{43} space during two harvest seasons. The BBOA and HOA + COA show similar low oxidative properties with varying f_{43}, which are located at the left-bottom of the triangular region during the summer and autumn harvest, respectively. This agrees well with the result observed by Crippa et al. (2013) in Paris. This further demonstrates that BBOA represents mainly the primary BBOA

during the harvests. As discussed above, OOA-BB could be associated to aged BBOA components with semi-volatile character in the BB plumes, which is the probably processed OOA from the BB emissions and/or emissions during specific burn phases (Weimer et al., 2008; Grieshop et al., 2009; Bougiatioti et al., 2014; Young et al., 2014). With the aging process in the atmosphere, OA clusters within a well-defined triangular region and shows more similar oxidative properties to OOA-BB and/or OOA (Fig. 12a). This implies that OOA-BB and/or BBOA might be further oxidized, and might be transformed into highly oxidized OOA. This result is also consistent with the studies of Jimenez et al. (2009) and Heringa et al. (2011).

Furthermore, the formation and transformation of primary and secondary BBOA during BB periods can be described by f_{44} vs. f_{60} plot (Cubison et al., 2011). In the f_{44} vs. f_{60} space of Figure 12b, OA shows a trend toward higher f_{44} and lower f_{60} values with the aging/dilution of BB plumes, appearing into the low-volatility OOA (LV-OOA) range. This is very consistent with previous reports in aircraft and laboratory studies (Cubison et al., 2011) with a similar trend. In a smog chamber experiment, Grieshop et al. (2009) also found that the relative contribution at *m/z* 44 and *m/z* 60 rapidly increases and decreases, respectively during aging process, which presents the characteristics of fresh and aged BBOA.

As increasing of the f_{44} / f_{60} ratio, the mass loadings of the PM_1 and OA show decreasing trends respectively (Fig. 12c − d), suggesting that the contribution of the fresh BB plume to the PM pollution gradually decreases with the aging of evolving ambient open BB plumes. Thus, it is reasonable to believe that the fresh BB plumes significantly contribute to the ambient OA burden during the harvest seasons. Logically, a decreasing trend of the OA / ΔCO ratio is presented with increasing of the f_{44} / f_{60} ratio (Fig. 12c − d), meaning that the BB emissions might be mixing with the regional and/or urban emissions as it is aging.

3.6 Impacts of various source regions on the PM pollution

Figure 13 presents the calculated air mass 48 h back trajectories (BTs) at 500 m arrival height above ground level at intervals of two hours (i.e. 00:00, 02:00, 04:00, …, 22:00) starting at CST using the HYSPLIT model (Draxler and Rolph, 2003) in Nanjing (118 °46'N, 32 °05'E). The corresponding BTs can be broadly classified into four principal clusters of air masses based on the spatial distributions during the summer and autumn harvests, respectively, i.e., northeasterly (NE) back-trajectories (BTs), easterly marine (EM) BTs, southeasterly marine (SEM) BTs, and southwesterly continental (SWC) for the summer harvest; northerly continental (NC) BTs, northeasterly marine (NEM) BTs, easterly marine (EM) BTs and southerly continental (SC) for the autumn harvest. The air masses in Nanjing in this study were mainly from the SEM BTs (accounting for 57.4% of all the BTs) during the summer harvest, while predominantly from the NC and EM BTs (at frequencies of 43.8% and 24%, respectively) during the autumn harvest (Fig. 13 and Table S3).

The total PM_1 loadings are on average the highest (71.3 μg m^{-3}) for a continental-related cluster (SWS BTs), which is almost twice higher than that of the lowest (24.4 μg m^{-3}) for the marine-related cluster (EM BTs) during the summer harvest. This suggests that the long-range transported pollutants from southwestern areas can cause the high PM pollution in the YRD region during the summer harvest. Similarly, the highest average concentration of PM_1 (80.9 μg m^{-3}) is associated with a continental-related cluster during the autumn harvest. Therefore, source regions are of utmost importance to the high air pollution in the YRD region during the harvest seasons.

The PM_1 chemical compositions show also significantly different fraction among the four clusters during the summer and autumn harvest respectively, which might be associated with the different source regions of air pollution. The contributions of BC, HOA + COA, and BB related OA (BBOA and OOA-BB) to PM_1 are rather high in the WC BTs, suggesting

618 a significant impact of local primary emissions and regional agricultural open fires (Figure S1)
619 on aerosol pollution in urban Nanjing during the summer harvest. The lowest PM_1 loadings
620 are associated with the EM BTs, but with the high contribution of HOA + COA during the
621 summer harvest. This suggests that the local sources play an important role in the relatively
622 low PM pollution during the summer harvest. For the NE BTs, the OOA, nitrate, and sulfate
623 account the high fractions of the total PM_1 mass, suggesting that regional pollution plays a
624 key role in controlling the PM pollution. Compared with other clusters during the autumn
625 harvest, the BB related emissions (e.g. BBOA, OOA-BB, and chloride) contribute the highest
626 fractions to the PM_1 mass in air masses originated from the SC BTs, indicating that BB
627 plumes potentially contribute to the highest pollution period during the summer harvest.
628 Apart from the high contributions of nitrate and OOA, HOA + COA also accounted a higher
629 fraction to PM_1 mass in the NEM and EM BTs than originated from the others during the
630 autumn harvest. These findings suggest that the marine-related BTs have the low levels of
631 background pollutants, which probably reflects the levels of local pollution. In addition, the
632 PM_1 components show the lowest concentrations for the NC BTs, compared to the other
633 clusters during the autumn harvest. When removing the mass concentrations of BB related
634 OA (BBOA and OOA-BB), the mean concentration of PM_1 (31.6 μg m^{-3}) for the NC BTs is
635 corresponding to a result (28.7 μg m^{-3}) for a similar cluster during a non-BB period (Huang
636 et al., 2012).
637
638 **4 Conclusions**
639 The characteristics, sources and evolution of atmospheric PM_1 species in urban Nanjing, the
640 YRD region of China were investigated using an Aerodyne ACSM during the two harvest
641 seasons, namely the summer wheat harvest (June 1 to 15, 2013) and the autumn rice harvest
642 (October 15 to 30, 2013). The PM_1 mass varies very dynamically for the two harvests,

ranging from 3.6 to 253.0 μg m^{-3} with a mean value of 38.16 μg m^{-3} during the summer harvest, and ranged from 7.3 to 163.6 μg m^{-3} with a mean value of 46.4 μg m^{-3} during the autumn harvest. The PM_1 species show a similar contribution, which on average account for 39% (41%) OA, 23% (20%) nitrate, 16% (14%) ammonium, 12% (11%) sulfate, 8% (13%) BC, and 1% (1%) chloride during the summer (autumn) harvest. Secondary inorganic species, i.e., nitrate, sulfate and ammonium, show highly similar diurnal patterns between the summer and autumn harvest, meaning its similar source emissions and chemical processing. In particular, OA, chloride and BC present higher concentrations in the diurnal cycles during the autumn harvest than during the summer harvest, due to larger impacts of BB and/or local primary emissions during the autumn harvest.

PMF analysis was performed on the ACSM OA mass spectra to investigate organic source apportionment during the two harvests. Four OA components were resolved including two POA factors associated with traffic and cooking (HOA + COA) and biomass burning OA (BBOA) emissions and two secondary factors associated with regional and highly oxidized OOA and less oxidized BB-like OA (OOA-BB). Apart from HOA + COA, BBOA and OOA-BB also present pronounced diurnal cycles during the harvests, with the highest concentrations occurring at night due to the nighttime BB plumes over urban Nanjing. This suggests that OOA-BB may be quickly oxidized a bit and condensed on the particle phase during the nighttime with the high RH and low *T* conditions. The diurnal profiles of OOA are similar to that of sulfate with relatively flat variations, reflecting their regional pollution. OA was dominated by secondary organics (OOA and OOA-BB) with the fraction more than 60% to total OA mass. POA shows a lower contribution to OA during the summer (autumn) harvest, traffic and cooking 15% (28%) and BB 7% (7%) emissions. The background level of f_{60} (0.26 ± 0.1%) was determined using the f_{44} vs. f_{60} space during the non-BB periods (in

July). Thus, we suggest a simpler method for estimating the fresh BBOA loadings based on the equation of BBOA = 15.1 × (*m/z* 60 – 0.26% × OA) during the harvests.

Generally, the (BBOA + OOA-BB) / ΔCO ratios decrease with the increasing of the f_{44}. The OA mass, however, decreases with the aging of BB plumes, implying that the fresh BB plumes play a key contribution to ambient OA burden during the harvest seasons. Air masses trajectory analysis indicates that local sources probably play an important role in the relatively low PM pollution associated with the air mass originated from the marine region during the harvests. However, the high PM pollution is mainly contributed by nitrate, BBOA, and OOA-BB, which is associated with air masses originated from the western (summer harvest) and southern (autumn harvest) areas.

Acknowledgements

This work was funded by the Natural Science Key Research of Jiangsu Province High Education (11KJA170002), the Foundation Research Project of Jiangsu Province (BK2012884, BK20140987), the Project Funded by the Jiangsu Province Science & Technology Support Program (BE2012771), the Environmental Monitoring Scientific Research Foundation of Jiangsu Province (1016), and the National Natural Science Foundation of China (21407080). We are very grateful for the help and support from Dr. Douglas R. Worsnop and Dr. John T. Jayne (Aerodyne Research Inc.) in the ACSM measurements. We also would like to thank Dr. P. Chen (Handix LLC) and Dr. W. Li (South Coast Air Quality Management District) for their constructive suggestions in improving the contents.

690 **References**

691 Aiken, A. C., Decarlo, P. F., Kroll, J. H., Worsnop, D. R., Huffman, J. A., Docherty, K. S.,
692 Ulbrich, I. M., Mohr, C., Kimmel, J. R., Sueper, D., Sun, Y., Zhang, Q., Trimborn, A.,
693 Northway, M., Ziemann, P. J., Canagaratna, M. R., Onasch, T. B., Alfarra, M. R., Prevot,
694 A. S. H., Dommen, J., Duplissy, J., Metzger, A., Baltensperger, U., and Jimenez, J. L.:
695 O/C and OM/OC ratios of primary, secondary, and ambient organic aerosols with
696 high-resolution time-of-flight aerosol mass spectrometry, Environ. Sci. Technol., 42,
697 4478–4485, 2008.

698 Aiken, A. C., Salcedo, D., Cubison, M. J., Huffman, J. A., DeCarlo, P. F., Ulbrich, I. M.,
699 Docherty, K. S., Sueper, D., Kimmel, J. R., Worsnop, D. R., Trimborn, A., Northway, M.,
700 Stone, E. A., Schauer, J. J., Volkamer, R. M., Fortner, E., de Foy, B., Wang, J., Laskin, A.,
701 Shutthanandan, V., Zheng, J., Zhang, R., Gaffney, J., Marley, N. A., Paredes-Miranda, G.,
702 Arnott, W. P., Molina, L. T., Sosa, G., and Jimenez, J. L.: Mexico City aerosol analysis
703 during MILAGRO using high resolution aerosol mass spectrometry at the urban
704 supersite (T0) – Part 1: Fine particle composition and organic source apportionment,
705 Atmos. Chem. Phys., 9, 6633-6653, doi:10.5194/acp-9-6633-2009, 2009.

706 Aiken, A. C., de Foy, B., Wiedinmyer, C., DeCarlo, P. F., Ulbrich, I. M., Wehrli, M. N.,
707 Szidat, S., Prévôt, A. S. H., Noda, J., Wacker, L., Volkamer, R., Fortner, E., Wang, J.,
708 Laskin, A., Shutthanandan, V., Zheng, J., Zhang, R., Paredes-Miranda, G., Arnott, W. P.,
709 Molina, L. T., Sosa, G., Querol, X., and Jimenez, J. L.: Mexico city aerosol analysis
710 during MILAGRO using high resolution aerosol mass spectrometry at the urban
711 supersite (T0) - Part 2: Analysis of the biomass burning contribution and the non-fossil
712 carbon fraction, Atmos. Chem. Phys., 10, 5315-5341, doi:10.5194/acp-10-5315-2010,
713 2010.

714 Alfarra, M. R., Prévôt, A. S. H., Szidat, S., Sandradewi, J., Weimer, S., Schreiber, D., Mohr,

M., and Baltensperger, U.: Identification of the mass spectral signature of organic aerosols from wood burning emissions, Environ. Sci Technol., 41, 5770-5777, 2007.

Allan, J. D., Bower, K. N., Coe, H., Boudries, H., Jayne, J. T., Canagaratna, M. R., Millet, D. B., Goldstein, A. H., Quinn, P. K., Weber, R. J., W. D. R.: Submicron aerosol composition at Trinidad Head, California, during ITCT 2K2: Its relationship with gas phase volatile organic carbon and assessment of instrument performance, J. Geophys. Res., 109: D23S24, 2004.

Allan, J. D., Williams, P. I., Morgan, W. T., Martin, C. L., Flynn, M. J., Lee, J., Nemitz, E., Phillips, G. J., Gallagher, M. W., and Coe, H.: Contributions from transport, solid fuel burning and cooking to primary organic aerosols in two UK cities, Atmos. Chem. Phys., 10, 647-668, doi:10.5194/acp-10-647-2010, 2010.

Andreae, M. O., and Merlet, P.: Emission of trace gases and aerosols from biomass burning, Global Biogeochem. Cycles, 15, 955-966, 2001.

Bougiatioti, A., Stavroulas, I., Kostenidou, E., Zarmpas, P., Theodosi, C., Kouvarakis, G., Canonaco, F., Prévôt, A. S. H., Nenes, A., Pandis, S. N., and Mihalopoulos, N.: Processing of biomass-burning aerosol in the eastern Mediterranean during summertime, Atmos. Chem. Phys., 14, 4793-4807, doi:10.5194/acp-14-4793-2014, 2014.

Canagaratna, M., Jayne, J., Jimenez, J. L., Allan, J. A., Alfarra, R., Zhang, Q., Onasch, T., Drewnick, F., Coe, H., Middlebrook, A., Delia, A., Williams, L., Trimborn, A., Northway, M., Kolb, C., Davidovits, P., and Worsnop, D.: Chemical and microphysical characterization of aerosols via Aerosol Mass Spectrometry, Mass Spectrom. Rev., 26, 185-222, 2007.

Canonaco, F., Crippa, M., Slowik, J. G., Baltensperger, U., and Prévôt, A. S. H.: SoFi, an IGOR-based interface for the efficient use of the generalized multilinear engine (ME-2)

739 for the source apportionment: ME-2 application to aerosol mass spectrometer data,
740 Atmos. Meas. Tech., 6, 3649-3661, doi:10.5194/amt-6-3649-2013, 2013.
741 Cheng, Y., Engling, G., He, K.-B., Duan, F.-K., Ma, Y.-L., Du, Z.-Y., Liu, J.-M., Zheng, M.,
742 and Weber, R. J.: Biomass burning contribution to Beijing aerosol, Atmos. Chem. Phys.,
743 13, 7765-7781, doi:10.5194/acp-13-7765-2013, 2013.
744 Crippa, M., DeCarlo, P. F., Slowik, J. G., Mohr, C., Heringa, M. F., Chirico, R., Poulain, L.,
745 Freutel, F., Sciare, J., Cozic, J., Di Marco, C. F., Elsasser, M., Nicolas, J. B.,
746 Marchand, N., Abidi, E., Wiedensohler, A., Drewnick, F., Schneider, J., Borrmann, S.,
747 Nemitz, E., Zimmermann, R., Jaffrezo, J.-L., Prévôt, A. S. H., and Baltensperger, U.:
748 Wintertime aerosol chemical composition and source apportionment of the organic
749 fraction in the metropolitan area of Paris, Atmos. Chem. Phys., 13, 961-981,
750 doi:10.5194/acp-13-961-2013, 2013.
751 Crippa, M., Canonaco, F., Lanz, V. A., Äijälä, M., Allan, J. D., Carbone, S., Capes, G.,
752 Ceburnis, D., Dall'Osto, M., Day, D. A., DeCarlo, P. F., Ehn, M., Eriksson, A., Freney, E.,
753 Hildebrandt Ruiz, L., Hillamo, R., Jimenez, J. L., Junninen, H., Kiendler-Scharr, A.,
754 Kortelainen, A.-M., Kulmala, M., Laaksonen, A., Mensah, A. A., Mohr, C., Nemitz, E.,
755 O'Dowd, C., Ovadnevaite, J., Pandis, S. N., Petäjä, T., Poulain, L., Saarikoski, S.,
756 Sellegri, K., Swietlicki, E., Tiitta, P., Worsnop, D. R., Baltensperger, U., and Prévôt, A. S.
757 H.: Organic aerosol components derived from 25 AMS data sets across Europe using a
758 consistent ME-2 based source apportionment approach, Atmos. Chem. Phys., 14,
759 6159-6176, doi:10.5194/acp-14-6159-2014, 2014.
760 Cubison, M. J., Ortega, A. M., Hayes, P. L., Farmer, D. K., Day, D., Lechner, M. J.,
761 Brune, W. H., Apel, E., Diskin, G. S., Fisher, J. A., Fuelberg, H. E., Hecobian, A.,
762 Knapp, D. J., Mikoviny, T., Riemer, D., Sachse, G. W., Sessions, W., Weber, R. J.,
763 Weinheimer, A. J., Wisthaler, A., and Jimenez, J. L.: Effects of aging on organic aerosol

764 from open biomass burning smoke in aircraft and laboratory studies, Atmos. Chem.
765 Phys., 11, 12049-12064, doi:10.5194/acp-11-12049-2011, 2011.
766 DeCarlo, P. F., Dunlea, E. J., Kimmel, J. R., Aiken, A. C., Sueper, D., Crounse, J.,
767 Wennberg, P. O., Emmons, L., Shinozuka, Y., Clarke, A., Zhou, J., Tomlinson, J.,
768 Collins, D. R., Knapp, D., Weinheimer, A. J., Montzka, D. D., Campos, T., and
769 Jimenez, J. L.: Fast airborne aerosol size and chemistry measurements above Mexico
770 City and Central Mexico during the MILAGRO campaign, Atmos. Chem. Phys., 8,
771 4027-4048, doi:10.5194/acp-8-4027-2008, 2008.
772 DeCarlo, P. F., Ulbrich, I. M., Crounse, J., de Foy, B., Dunlea, E. J., Aiken, A. C., Knapp, D.,
773 Weinheimer, A. J., Campos, T., Wennberg, P. O., and Jimenez, J. L.: Investigation of the
774 sources and processing of organic aerosol over the Central Mexican Plateau from
775 aircraft measurements during MILAGRO, Atmos. Chem. Phys., 10, 5257-5280,
776 doi:10.5194/acp-10-5257-2010, 2010.
777 de Gouw, J. A., Middlebrook, A. M., Warneke, C., Goldan, P. D., Kuster, W. C., Roberts, J.
778 M., Fehsenfeld, F. C., Worsnop, D. R., Canagaratna, M. R., Pszenny, A. A. P., Keene, W.
779 C., Marchewka, M., Bertman, S. B., and Bates, T. S.: Budget of organic carbon in a
780 polluted atmosphere: Results from the New England Air Quality Study in 2002, J.
781 Geophys. Res. Atmos., 110, D16305, 2005.
782 Ding, A. J., Fu, C. B., Yang, X. Q., Sun, J. N., Petäjä, T., Kerminen, V.-M., Wang, T., Xie, Y.,
783 Herrmann, E., Zheng, L. F., Nie, W., Liu, Q., Wei, X. L., and Kulmala, M.: Intense
784 atmospheric pollution modifies weather: a case of mixed biomass burning with fossil
785 fuel combustion pollution in eastern China, Atmos. Chem. Phys., 13, 10545-10554,
786 doi:10.5194/acp-13-10545-2013, 2013.

787 Draxler, R. R., Rolph, G. D.: HYSPLIT (HYbrid Single-Particle Lagrangian Integrated
788 Trajectory) Model Access via NOAA ARL READY Website. NOAA Air Resources
789 Laboratory, Silver Spring, MD. http://www.arl.noaa.gov/ready/hysplit4.html, 2003.
790 Du, H. H., Kong, L.D., Cheng, T.T., Chen, J.M., Du, J.F., Li, L., Xia, X.G., Leng, C.P., Huang,
791 G. H.: Insights into summertime haze pollution events over Shanghai based on online
792 water-soluble ionic composition of aerosols, Atmos. Environ., 45, 5131-5137, 2011.
793 Ge, W. Z., Chen, R. J., Song, W. M., and Kan, H. D.: Daily Visibility and Hospital Admission
794 in Shanghai, China, Biomed Environ. Sci., 24(2): 117-121, 2011.
795 Gilardoni, S., Liu, S., Takahama, S., Russell, L. M., Allan, J. D., Steinbrecher, R., Jimenez, J.
796 L., De Carlo, P. F., Dunlea, E. J., and Baumgardner, D.: Characterization of organic
797 ambient aerosol during MIRAGE 2006 on three platforms, Atmos. Chem. Phys., 9,
798 5417-5432, doi:10.5194/acp-9-5417-2009, 2009.
799 Grieshop, A. P., Donahue, N. M., and Robinson, A. L.: Laboratory investigation of
800 photochemical oxidation of organic aerosol from wood fires 2: analysis of aerosol mass
801 spectrometer data, Atmos. Chem. Phys., 9, 2227-2240, doi:10.5194/acp-9-2227-2009,
802 2009.
803 He, L.-Y., Lin, Y., Huang, X.-F., Guo, S., Xue, L., Su, Q., Hu, M., Luan, S.-J., and
804 Zhang, Y.-H.: Characterization of high-resolution aerosol mass spectra of primary
805 organic aerosol emissions from Chinese cooking and biomass burning, Atmos. Chem.
806 Phys., 10, 11535-11543, doi:10.5194/acp-10-11535-2010, 2010.
807 Healy, R. M., Sciare, J., Poulain, L., Crippa, M., Wiedensohler, A., Prévôt, A. S. H.,
808 Baltensperger, U., Sarda-Estève, R., McGuire, M. L., Jeong, C.-H., McGillicuddy, E.,
809 O'Connor, I. P., Sodeau, J. R., Evans, G. J., and Wenger, J. C.: Quantitative
810 determination of carbonaceous particle mixing state in Paris using single-particle mass

spectrometer and aerosol mass spectrometer measurements, Atmos. Chem. Phys., 13, 9479-9496, doi:10.5194/acp-13-9479-2013, 2013.

Heringa, M. F., DeCarlo, P. F., Chirico, R., Tritscher, T., Dommen, J., Weingartner, E., Richter, R., Wehrle, G., Prévôt, A. S. H., and Baltensperger, U.: Investigations of primary and secondary particulate matter of different wood combustion appliances with a high-resolution time-of-flight aerosol mass spectrometer, Atmos. Chem. Phys., 11, 5945-5957, doi:10.5194/acp-11-5945-2011, 2011.

Hu, W. W., Hu, M., Yuan, B., Jimenez, J. L., Tang, Q., Peng, J. F., Hu, W., Shao, M., Wang, M., Zeng, L. M., Wu, Y. S., Gong, Z. H., Huang, X. F., and He, L. Y.: Insights on organic aerosol aging and the influence of coal combustion at a regional receptor site of central eastern China, Atmos. Chem. Phys., 13, 10095-10112, doi:10.5194/acp-13-10095-2013, 2013.

Huang, X.-F., He, L.-Y., Hu, M., Canagaratna, M. R., Sun, Y., Zhang, Q., Zhu, T., Xue, L., Zeng, L.-W., Liu, X.-G., Zhang, Y.-H., Jayne, J. T., Ng, N. L., and Worsnop, D. R.: Highly time-resolved chemical characterization of atmospheric submicron particles during 2008 Beijing Olympic Games using an Aerodyne High-Resolution Aerosol Mass Spectrometer, Atmos. Chem. Phys., 10, 8933-8945, doi:10.5194/acp-10-8933-2010, 2010.

Huang, X.-F., He, L.-Y., Hu, M., Canagaratna, M. R., Kroll, J. H., Ng, N. L., Zhang, Y.-H., Lin, Y., Xue, L., Sun, T.-L., Liu, X.-G., Shao, M., Jayne, J. T., and Worsnop, D. R.: Characterization of submicron aerosols at a rural site in Pearl River Delta of China using an Aerodyne High-Resolution Aerosol Mass Spectrometer, Atmos. Chem. Phys., 11, 1865-1877, doi:10.5194/acp-11-1865-2011, 2011.

Huang, X.-F., He, L.-Y., Xue, L., Sun, T.-L., Zeng, L.-W., Gong, Z.-H., Hu, M., and Zhu, T.: Highly time-resolved chemical characterization of atmospheric fine particles during

836 2010 Shanghai World Expo, Atmos. Chem. Phys., 12, 4897-4907,
837 doi:10.5194/acp-12-4897-2012, 2012.
838 Huang, X.-F., Xue, L., Tian, D.-X., Shao, W.-W., Sun, T.-L., Gong, Z.-H., Ju, W.-W., Jiang,
839 B., Hu, M., and He, L.-Y.: Highly time-resolved carbonaceous aerosol characterization
840 in Yangtze River Delta of China: Composition, mixing state and secondary formation,
841 Atmos. Environ., 64, 200-207, 2013.
842 Huffman, J. A., Docherty, K. S., Aiken, A. C., Cubison, M. J., Ulbrich, I. M., DeCarlo, P. F.,
843 Sueper, D., Jayne, J. T., Worsnop, D. R., Ziemann, P. J., and Jimenez, J. L.:
844 Chemically-resolved aerosol volatility measurements from two megacity field studies,
845 Atmos. Chem. Phys., 9, 7161-7182, doi:10.5194/acp-9-7161-2009, 2009.
846 Jimenez, J. L., Canagaratna, M. R., Donahue, N. M., Prévôt, A. S. H., Zhang, Q., Kroll, J. H.,
847 DeCarlo, P. F., Allan, J. D., Coe, H., Ng, N. L., Aiken, A. C., Docherty, K. S., Ulbrich, I.
848 M., Grieshop, A. P., Robinson, A. L., Duplissy, J., Smith, J. D., Wilson, K. R., Lanz, V.
849 A., Hueglin, C., Sun, Y. L., Tian, J., Laaksonen, A., Raatikainen, T., Rautiainen, J.,
850 Vaattovaara, P., Ehn, M., Kulmala, M., Tomlinson, J. M., Collins, D. R., Cubison, M. J.,
851 E, Dunlea, J., Huffman, J. A., Onasch, T. B., Alfarra, M. R., Williams, P. I., Bower, K.,
852 Kondo, Y., Schneider, J., Drewnick, F., Borrmann, S., Weimer, S., Demerjian, K.,
853 Salcedo, D., Cottrell, L., Griffin, R., Takami, A., Miyoshi, T., Hatakeyama, S., Shimono,
854 A., Sun, J. Y., Zhang, Y. M., Dzepina, K., Kimmel, J. R., Sueper, D., Jayne, J. T.,
855 Herndon, S. C., Trimborn, A. M., Williams, L. R., Wood, E. C., Middlebrook, A. M.,
856 Kolb, C. E., Baltensperger, U., and Worsnop, D. R.: Evolution of organic aerosols in the
857 atmosphere, Science, 326, 1525-1529, 2009.
858 Justice, C. O., Giglio, L., Korontzi, S., Owens, J., Morisette, J.T., Roy, D., Descloitres, J.,
859 Alleaume, S., Petitcolin, F., Kaufman, Y.: The MODIS fire products, Remote Sens.
860 Environ., 83, 244-262, 2002.

Kaufman, Y. J., Tanre, D., and Boucher, O.: A satellite view of aerosols in the climate system, Nature, 419: 215-23, 2002.

Kaufman, Y. J., Ichoku, C., Giglio, L., Korontzi, S., Chu, D. A., Hao, W. M., Li R. R., Justice, C. O.: Fire and smoke observed from the Earth Observing System MODIS instrument-products, validation, and operational use, Int. J. Remote Sensing, 24, 1765-781, 2003.

Kawamura, K., Tachibana, E., Okuzawa, K., Aggarwal, S. G., Kanaya, Y., and Wang, Z. F.: High abundances of water-soluble dicarboxylic acids, ketocarboxylic acids and α-dicarbonyls in the mountaintop aerosols over the North China Plain during wheat burning season, Atmos. Chem. Phys., 13, 8285-8302, doi:10.5194/acp-13-8285-2013, 2013.

Lanz, V. A., Alfarra, M. R., Baltensperger, U., Buchmann, B., Hueglin, C., and Prévôt, A. S. H.: Source apportionment of submicron organic aerosols at an urban site by factor analytical modelling of aerosol mass spectra, Atmos. Chem. Phys., 7, 1503-1522, doi:10.5194/acp-7-1503-2007, 2007.

Lathem, T. L., Beyersdorf, A. J., Thornhill, K. L., Winstead, E. L., Cubison, M. J., Hecobian, A., Jimenez, J. L., Weber, R. J., Anderson, B. E., and Nenes, A.: Analysis of CCN activity of Arctic aerosol and Canadian biomass burning during summer 2008, Atmos. Chem. Phys., 13, 2735-2756, doi:10.5194/acp-13-2735-2013, 2013.

Lee, T., Sullivan, A. P., Mack, L., Jimenez, J. L., Kreidenweis, S. M., Onasch, T. B., Worsnop, D. R., Malm, W., Wold, C. E., Hao, W. M., and Collett, J. L.: Chemical smoke marker emissions during flaming and smoldering phases of laboratory open burning of wildland fuels, Aerosol Sci. Tech., 44, 1-5, 2010.

Li, X. H., Wang, S. X., Duan, L., Hao, J. M., Li, Y. S., and Yang, L.: Particulate and trace gas emissions from open burning of wheat straw and corn stover in China, Environ. Sci. Technol., 41 (17): 6052-6058, 2007.

Lipsky, E. M. and Robinson, A. L.: Effects of dilution on fine particle mass and partitioning of semivolatile organics in diesel exhaust and wood smoke, Environ. Sci. Technol., 40, 155–162, 2006.

Liu, D., Allan, J., Corris, B., Flynn, M., Andrews, E., Ogren, J., Beswick, K., Bower, K., Burgess, R., Choularton, T., Dorsey, J., Morgan, W., Williams, P. I., and Coe, H.: Carbonaceous aerosols contributed by traffic and solid fuel burning at a polluted rural site in Northwestern England, Atmos. Chem. Phys., 11, 1603-1619, doi:10.5194/acp-11-1603-2011, 2011.

Liu, D., Allan, J. D., Young, D. E., Coe, H., Beddows, D., Fleming, Z. L., Flynn, M. J., Gallagher, M. W., Harrison, R. M., Lee, J., Prevot, A. S. H., Taylor, J. W., Yin, J., Williams, P. I., and Zotter, P.: Size distribution, mixing state and source apportionments of black carbon aerosols in London during winter time, Atmos. Chem. Phys. Discuss., 14, 16291-16349, doi:10.5194/acpd-14-16291-2014, 2014.

Maenhaut, W., Vermeylen, R., Claeys, M., Vercauteren, J., Matheeussen, C., Roekens, E.: Assessment of the contribution from wood burning to the PM_{10} aerosol in Flanders, Belgium, Sci. Total Environ., 437, 226-236, 2012.

Middlebrook, A. M., Bahreini, R., Jimenez, J. L., and Canagaratna, M. R.: Evaluation of composition-dependent collection efficiencies for the aerodyne aerosol mass spectrometer using field data, Aerosol Sci. Tech., 46, 258-271, 2011.

Mohr, C., Huffman, J. A., Cubison, M. J., Aiken, A. C., Docherty, K. S., Kimmel, J. R., Ulbrich, I. M., Hannigan, M., and Jimenez, J. L.: Characterization of primary organic aerosol emissions from meat cooking, trash burning, and motor vehicles with

909 High-Resolution Aerosol Mass Spectrometry and comparison with ambient and chamber
910 observations, Environ. Sci. Technol., 43, 2443-2449, 2009.
911 Mohr, C., DeCarlo, P. F., Heringa, M. F., Chirico, R., Slowik, J. G., Richter, R., Reche, C.,
912 Alastuey, A., Querol, X., Seco, R., Peñuelas, J., Jiménez, J. L., Crippa, M.,
913 Zimmermann, R., Baltensperger, U., and Prévôt, A. S. H.: Identification and
914 quantification of organic aerosol from cooking and other sources in Barcelona using
915 aerosol mass spectrometer data, Atmos. Chem. Phys., 12, 1649-1665,
916 doi:10.5194/acp-12-1649-2012, 2012.
917 Ng, N. L., Canagaratna, M. R., Zhang, Q., Jimenez, J. L., Tian, J., Ulbrich, I. M., Kroll, J. H.,
918 Docherty, K. S., Chhabra, P. S., Bahreini, R., Murphy, S. M., Seinfeld, J. H.,
919 Hildebrandt, L., Donahue, N. M., DeCarlo, P. F., Lanz, V. A., Prévôt, A. S. H., Dinar, E.,
920 Rudich, Y., and Worsnop, D. R.: Organic aerosol components observed in Northern
921 Hemispheric datasets from aerosol mass spectrometry, Atmos. Chem. Phys., 10,
922 4625-4641, doi:10.5194/acp-10-4625-2010, 2010.
923 Ng, N. L., Herndon, S. C., Trimborn, A., Canagaratna, M. R., Croteau, P. L., Onasch, T. B.,
924 Sueper, D., Worsnop, D. R., Zhang, Q., Sun, Y. L., and Jayne, J. T.: An aerosol chemical
925 speciation monitor (ACSM) for routine monitoring of the composition and mass
926 concentrations of ambient aerosol, Aerosol Sci. Technol., 45: 7, 770 -784, 2011a.
927 Ng, N. L., Canagaratna, M. R., Jimenez, J. L., Chhabra, P. S., Seinfeld, J. H., and
928 Worsnop, D. R.: Changes in organic aerosol composition with aging inferred from
929 aerosol mass spectra, Atmos. Chem. Phys., 11, 6465-6474,
930 doi:10.5194/acp-11-6465-2011, 2011b.
931 Ng, N. L., Canagaratna, M. R., Jimenez, J. L., Zhang, Q., Ulbrich, I. M., and Worsnop, D. R.:
932 Real-time methods for estimating organic component mass concentrations from aerosol
933 mass spectrometer data, Environ. Sci. Technol., 45, 910-916, 2011c.

Paatero, P.: Least squares formulation of robust non-negative factor analysis, Chemom. Intell. Lab. Syst., 37, 23-35, 1997.

Paatero, P.: The multilinear engine – A table-driven, least squares program for solving multilinear problems, including the n-way parallel factor analysis model, J. Comput. Graph. Stat., 8, 854–888, 1999.

Reche, C., Viana, M., Amato, F., Alastuey, A., Moreno, T., Hillamo, R., Teinila, K., Saarnio, K., Seco, R., Penuelas, J., Mohr, C., Prévôt, A. S. H., and Querol, X,.: Biomass burning contributions to urban aerosols in a coastal Mediterranean City, Sci. Total Environ., 427, 175-190, 2012.

Robinson, A. L., Donahue, N. M., Shrivastava, M. K., Weitkamp, E. A., Sage, A. M., Grieshop, A. P., Lane, T. E., Pierce, J. R., and Pandis, S. N.: Rethinking organic aerosols: Semivolatile emissions and photochemical aging, Science, 315, 1259–1262, doi:10.1126/science.1133061, 2007.

Sandradewi, J., Prevot, A. S. H., Szidat, S., Perron, N., Alfarra, M. R., Lanz, V. A., Weingartner, E., and Baltensperger, U.: Using aerosol light absorption measurements for the quantitative determination of wood burning and traffic emission contributions to particulate matter, Environ. Sci. Technol., 42, 3316–3323, 2008.

Sun, J. Y., Zhang, Q., Canagaratna, M. R., Zhang, Y. M., Ng, N. L., Sun, Y. L., Jayne, J. T., Zhang, X. C., Zhang, X. Y., and Worsnop, D. R.: Highly time-and size-resolved characterization of submicron aerosol particles in Beijing using an Aerodyne Aerosol Mass Spectrometer, Atmos. Environ., 44, 131-140, 2010.

Sun, Y.-L., Zhang, Q., Schwab, J. J., Demerjian, K. L., Chen, W.-N., Bae, M.-S., Hung, H.-M., Hogrefe, O., Frank, B., Rattigan, O. V., and Lin, Y.-C.: Characterization of the sources and processes of organic and inorganic aerosols in New York city with a high-resolution

time-of-flight aerosol mass apectrometer, Atmos. Chem. Phys., 11, 1581-1602, doi:10.5194/acp-11-1581-2011, 2011a.

Sun, Y. L., Zhang, Q., Schwab, J. J., Chen, W. N., Bae, M. S., Lin, Y. C., Hung, H. M., and Demerjian, K. L.: A case study of aerosol processing and evolution in summer in New York City, Atmos. Chem. Phys., 11, 12737-12750, doi:10.5194/acp-11-12737-2011, 2011b.

Sun, Y. L., Wang, Z. F., Dong, H. B., Yang, T., Li, J., Pan, X. L., Chen, P., and Jayne, J. T.: Characterization of summer organic and inorganic aerosols in Beijing, China with an Aerosol Chemical Speciation Monitor, Atmos. Environ., 51, 250-259, 2012.

Sun, Y. L., Wang, Z. F., Fu, P. Q., Yang, T., Jiang, Q., Dong, H. B., Li, J., and Jia, J. J.: Aerosol composition, sources and processes during wintertime in Beijing, China, Atmos. Chem. Phys., 13, 4577-4592, doi:10.5194/acp-13-4577-2013, 2013.

Takegawa, N., Miyakawa, T., Kondo, Y., Jimenez, J. L., Zhang, Q., Worsnop, D. R., and Fukuda, M.: Seasonal and diurnal variations of submicron organic aerosol in Tokyo observed using the Aerodyne aerosol mass spectrometer, J. Geophys. Res., 111, D11206, 2006.

Ulbrich, I. M., Canagaratna, M. R., Zhang, Q., Worsnop, D. R., and Jimenez, J. L.: Interpretation of organic components from Positive Matrix Factorization of aerosol mass spectrometric data, Atmos. Chem. Phys., 9, 2891–2918, doi:10.5194/acp-9-2891-2009, 2009.

Wang, G. H., Kawamura, K., Xie, M. J., Hu, S. Y., Cao, J. J., An, Z. H., Waston J. G., and Chow, J. C.: Organic molecular compositions and size distributions of Chinese summer and autumn aerosols from Nanjing: characteristic haze event caused by wheat straw burning, Environ. Sci. Technol., 43 (17): 6493-6499, 2009a.

Wang, Y. Q., Zhang, X. Y., and Draxler, R. R.: TrajStat: GIS-based software that uses various trajectory statistical analysis methods to identify potential sources from long-term air pollution measurement data, Environ. Modell. Softw., 24: 938-939, 2009b.

Watson, J. G.: Visibility: Science and regulation, J. Air Waste Manage. Assoc., 52, 628-713, 2002.

Weimer, S., Alfarra, M. R., Schreiber, D., Mohr, M., Prévôt, A. S. H., and Baltensperger, U.: Organic aerosol mass spectral signatures from wood-burning emissions: Influence of burning conditions and wood type, J. Geophys. Res., 113, D10304, doi:10.1029/2007JD009309, 2008.

Yee, L. D., Kautzman, K. E., Loza, C. L., Schilling, K. A., Coggon, M. M., Chhabra, P. S., Chan, M. N., Chan, A. W. H., Hersey, S. P., Crounse, J. D., Wennberg, P. O., Flagan, R. C., and Seinfeld, J. H.: Secondary organic aerosol formation from biomass burning intermediates: phenol and methoxyphenols, Atmos. Chem. Phys., 13, 8019-8043, doi:10.5194/acp-13-8019-2013, 2013.

Young, D. E., Allan, J. D., Williams, P. I., Green, D. C., Harrison, R. M., Yin, J., Flynn, M. J., Gallagher, M. W., and Coe, H.: Investigating the two-component model of solid fuel organic aerosol in London: processes, PM_1 contributions, and seasonality, Atmos. Chem. Phys. Discuss., 14, 20845-20882, doi:10.5194/acpd-14-20845-2014, 2014.

Zhang, H., Ye, X., Cheng, T., Chen, J., Yang, X., Wang, L., Zhang, R.: A laboratory study of agricultural crop residue combustion in China: Emission factors and emission inventory, Atmos. Environ., 42, 8432-8441, 2008.

Zhang, Q., Worsnop, D. R., Canagaratna, M. R., and Jimenez, J. L.: Hydrocarbon-like and oxygenated organic aerosols in Pittsburgh: insights into sources and processes of organic aerosols, Atmos. Chem. Phys., 5, 3289-3311, doi:10.5194/acp-5-3289-2005, 2005a.

Zhang, Q., Alfarra, M.R. Worsnop, D., Allan, J. D., Coe, H., Cangaratna, M. R., Jimenez, J. L.: Deconvolution and quantification of hydrocarbon-like and oxygenated organic aerosols based on aerosol mass spectrometry, Environ. Sci. Technol., 39, 4938-4952, 2005b.

Zhang, Q., Jimenez, J. L., Canagaratna, M. R., Allan, J. D, Coe, H., Ulbrich, I. M., Alfarra, M. R., Takami, A., Middlebrook, A. M., Sun, Y. L., Dzepina, K., Dunlea, E., Docherty, K., DeCarlo, P, F., Salcedo, D., Onasch, T., Jayne, J. T., Miyoshi, T., Shimono, A., Hatakeyama, S., Takegawa, N., Kondo, Y., Schneider, J., Drewnick, F., Borrmann, S., Weimer, S., Demerjian, K., Williams, P., Bower, K., Bahreini, R., Cottrell, L., Griffin, R. J., Rautiainen, J., Sun, J. Y., Zhang, Y. M., Worsnop, D. R.: Ubiquity and dominance of oxygenated species in organic aerosols in anthropogenically-influenced Northern Hemisphere midlatitudes, Geophys. Res. Lett., 34(13): L13801, 2007.

Zhang, Q., Jimenez, J. L., Canagaratna, M. R., Ulbrich, I. M., Ng, N. L., Worsnop, D. R., Sun, Y. L.: Understanding atmospheric organic aerosols via factor analysis of aerosol mass spectrometry: a review, Anal. Bioanal. Chem., 401:3045-3067, 2011.

1022 Table 1

1023 Mean mass concentration of PM_1 (NR-PM_1 + BC) (μg m^{-3}) and standard deviation (S.D.) during the

1024 harvest seasons.

Species	Summer harvest		Autumn harvest	
	Mean	S.D.	Mean	S.D.
NO_3	9.0	7.1	9.2	6.2
SO_4	5.0	2.4	4.7	2.5
NH_4	7.0	3.5	6.4	3.5
Chl	0.4	0.9	0.7	0.8
OA	15.4	12.8	22.3	17.5
BC	3.2	2.2	6.0	3.8
PM_1	38.5	24.3	46.4	27.0
HOA + COA	2.2	2.4	5.7	7.6
BBOA	1.1	1.0	1.5	1.6
OOA-BB	4.1	4.6	6.5	7.3
OOA	7.1	3.6	6.6	3.2

1025

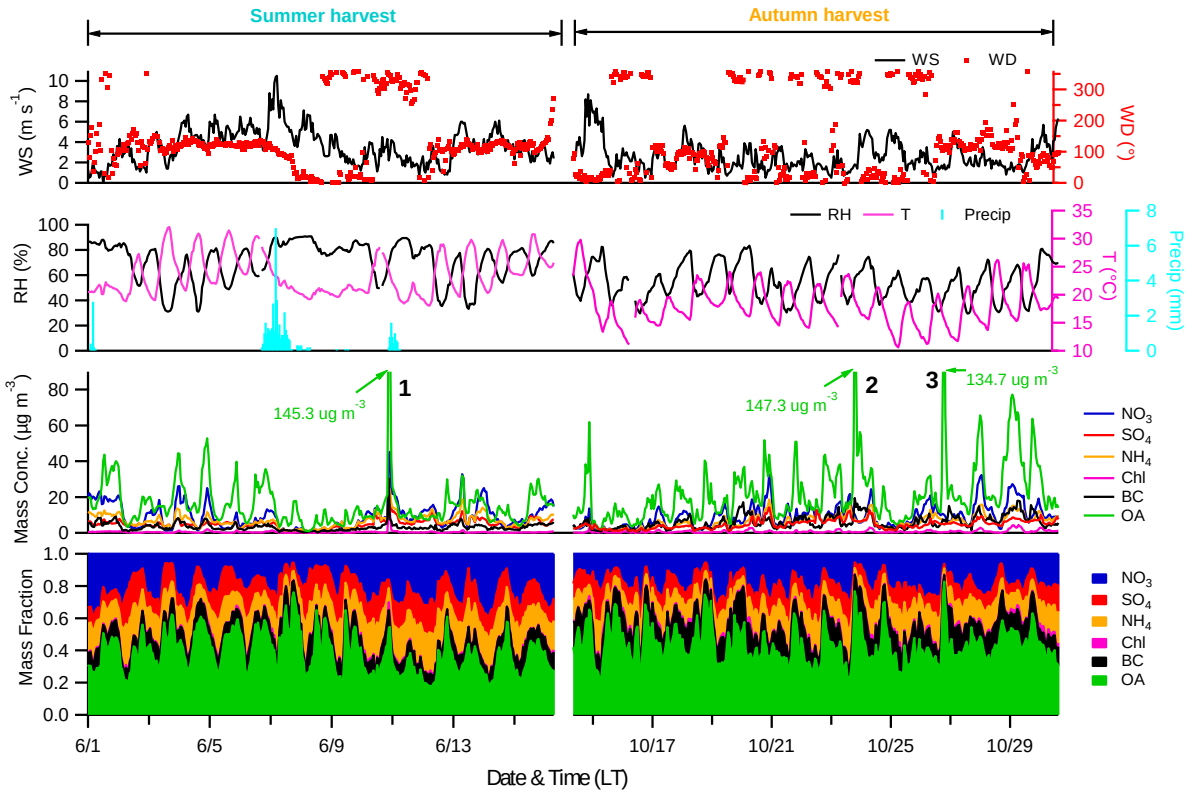

Fig. 1. Time series of **(a)** wind speed (WS) and wind direction (WD); **(b)** relative humidity (RH), temperature (*T*) and precipitation (Precip); **(c)** submicron aerosol species, i.e., organic aerosol (OA), ammonium (NH_4), nitrate (NO_3), sulfate (SO_4), chloride (Chl) and black carbon (BC); and **(d)** mass fraction during the harvest seasons. Three case events are marked and discussed in the text.

1031

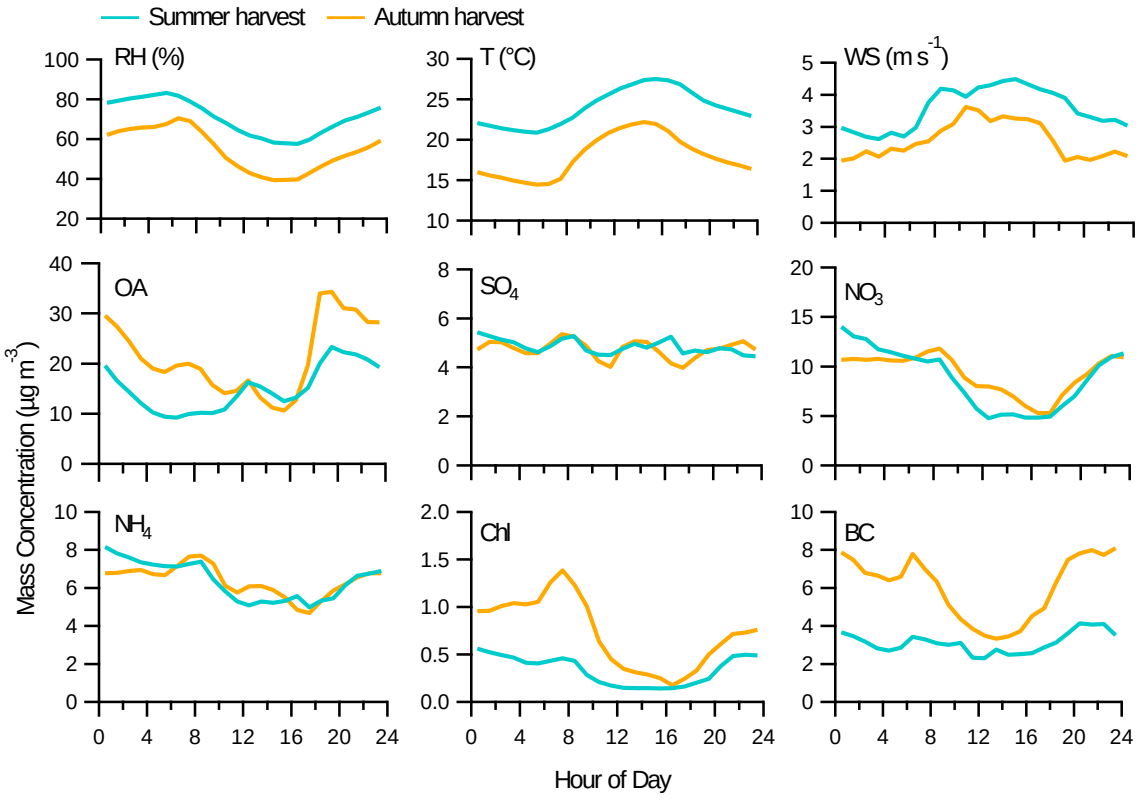

1032

1033 **Fig. 2.** Diurnal variation patterns of meteorological factors (i.e. RH, *T*, and WS), PM_1 species including

1034 organic aerosol (OA), nitrate (NO_3), sulfate (SO_4), ammonium (NH_4), chloride (Chl), and black carbon

1035 (BC) during the harvest seasons.

1036

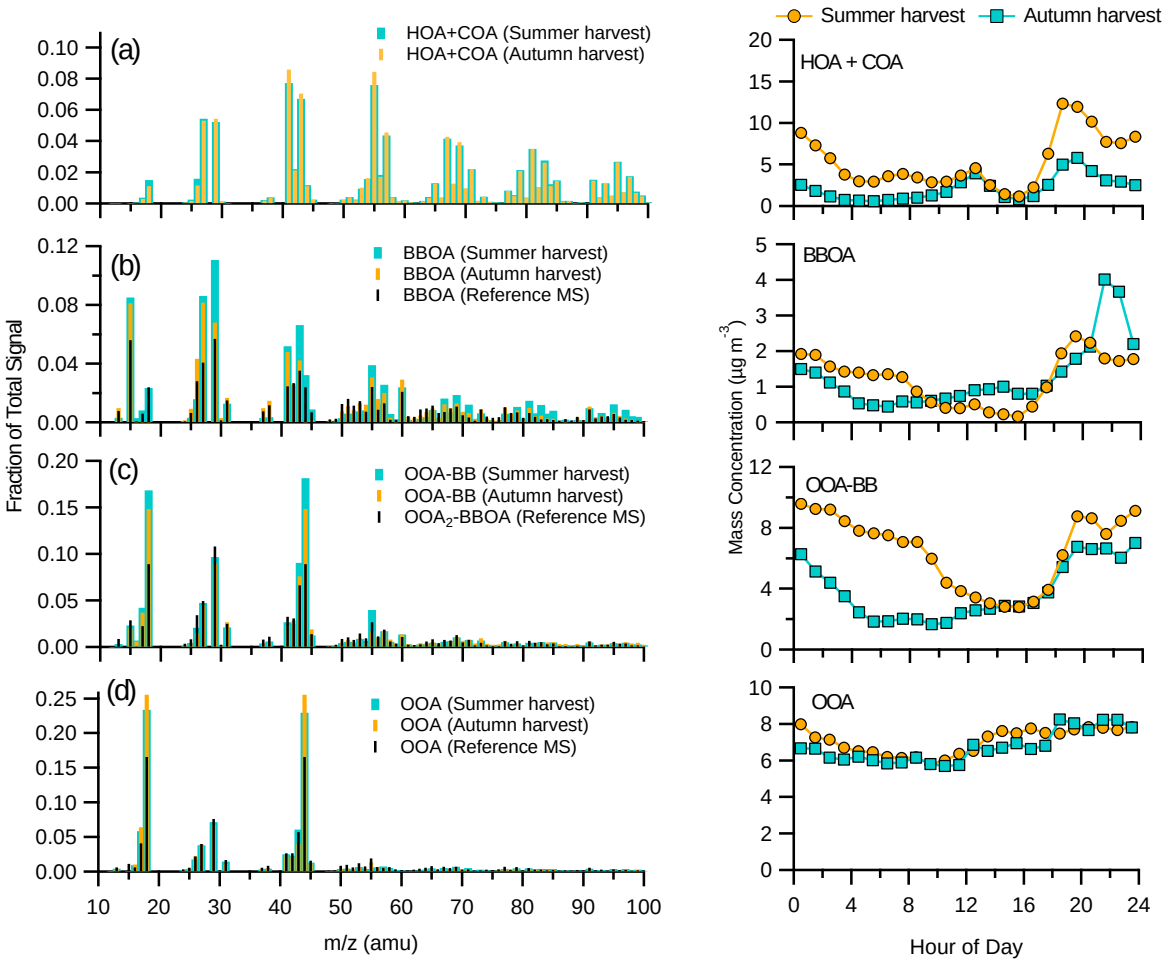

Fig. 3. Mass spectra profiles (left) and diurnal variations (right) of four OA factors, i.e., hydrocarbon-like and cooking-emission related OA (HOA + COA), fresh biomass burning (BB) OA (BBOA), oxygenated BB-influenced OA (OOA-BB), and highly oxygenated OA (OOA). Note that: reference mass spectra (MS) are obtained from the results by Crippa et al. (2013), and oxygenated BBOA components have been resolved (OOA_2-BBOA).

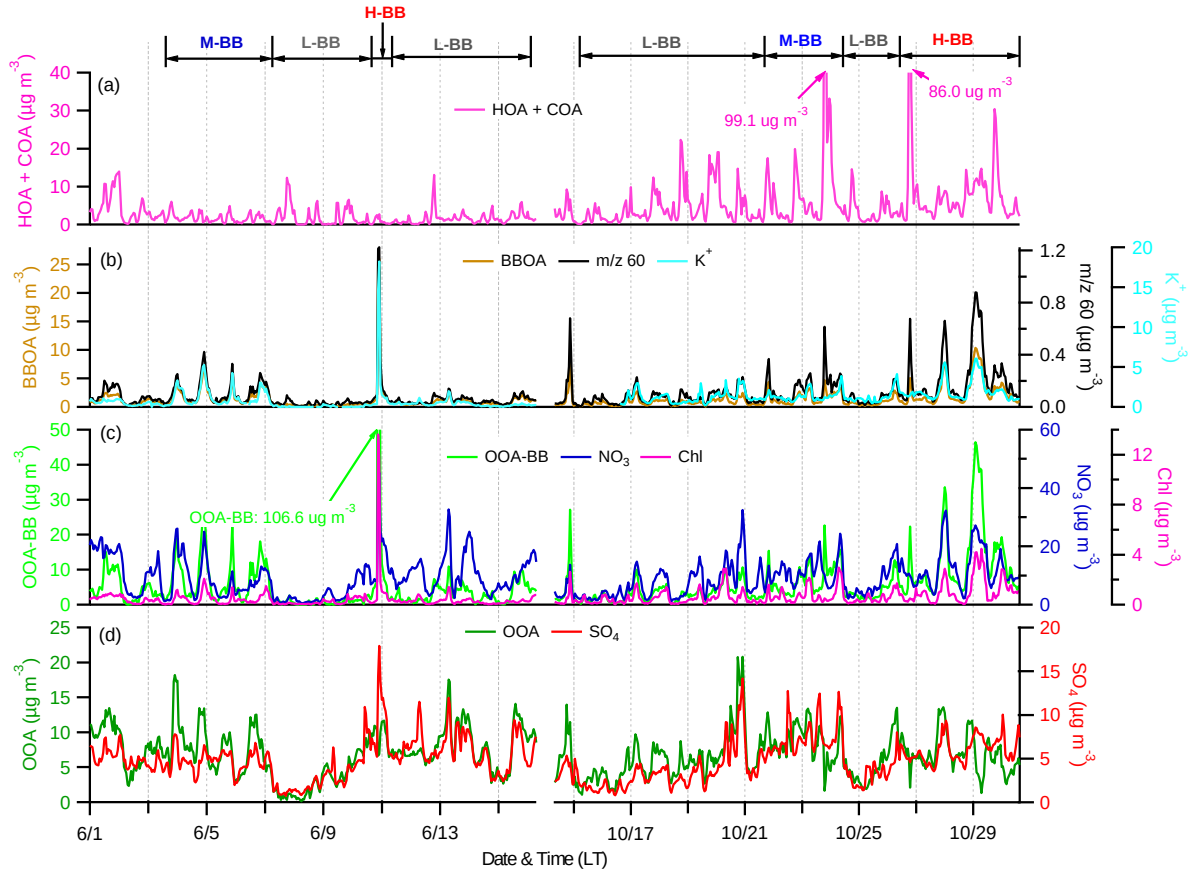

Fig. 4. Time series of OA factors (left) and relevant tracer species (right): **(a)** HOA + COA; **(b)** BBOA and a surrogate of levoglucosan (*m/z* 60) and potassium ion (K^+); **(c)** OOA-BB, nitrate and chloride; **(d)** OOA and SO_4. Note that different BBOA mass concentrations for low biomass burning period (L-BB), medium biomass burning period (M-BB), and high biomass burning period (H-BB).

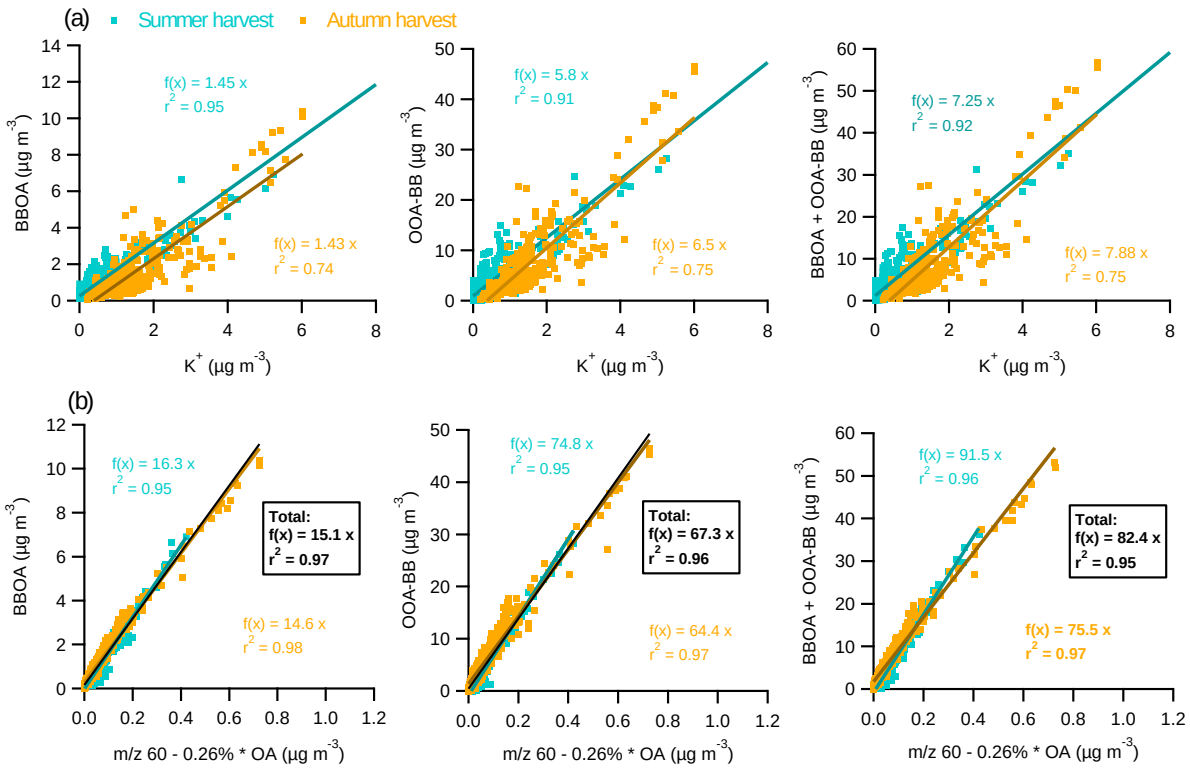

Fig. 5. Comparison of biomass burning-related PMF factors (BBOA and OOA-BB) and biomass related species: **(a)** K^+; and **(b)** the ACSM *m/z* 60 minus 0.26% × OA (applied metric of background f_{60} = 0.26 % of OA is discussed in the section 3.4 of the text) during the summer and autumn harvest.

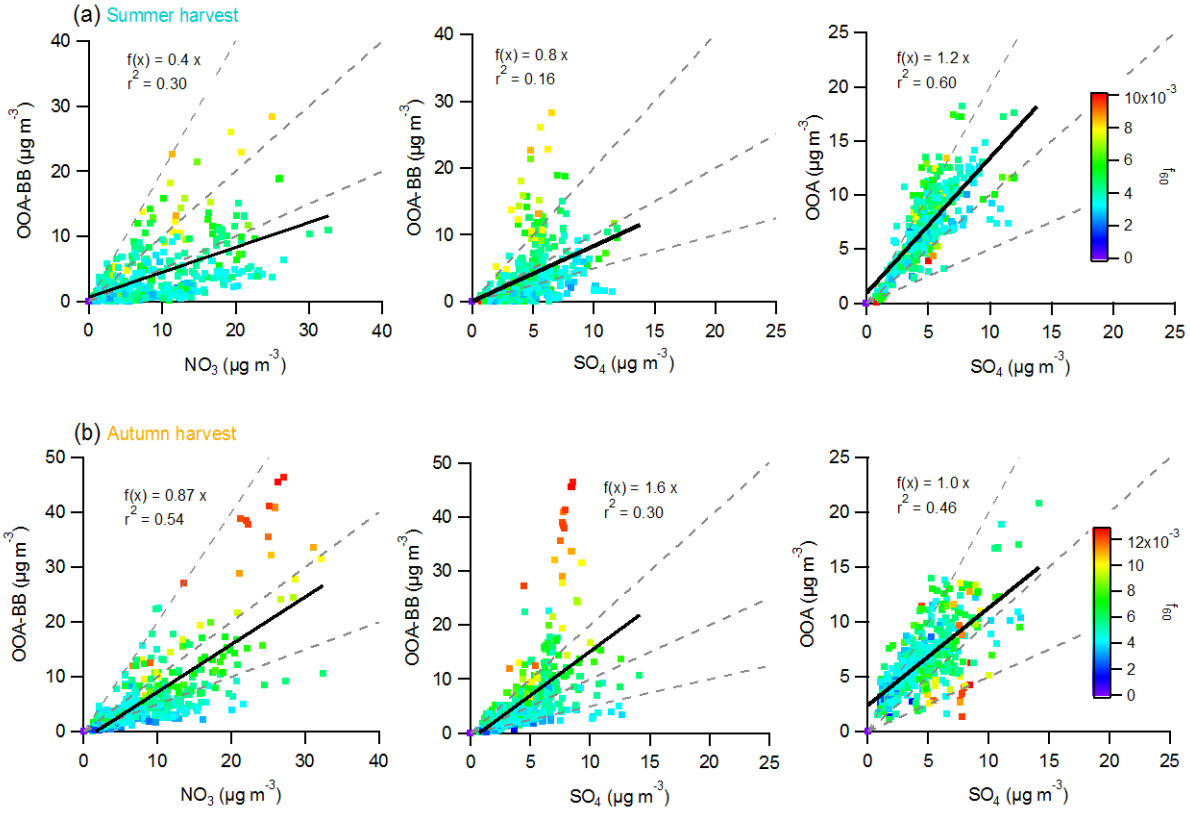

Fig. 6. Comparison of two kinds of oxygenated OA (OOA-BB and OOA) and two kinds of secondary inorganic species, i.e., nitrate (NO_3) and sulfate (SO_4), during the harvest seasons. Colored by the f_{60} as a biomass-burning marker. The three dashed lines in the plot refer to 2 : 1, 1 : 1, and 1 : 2 lines, respectively.

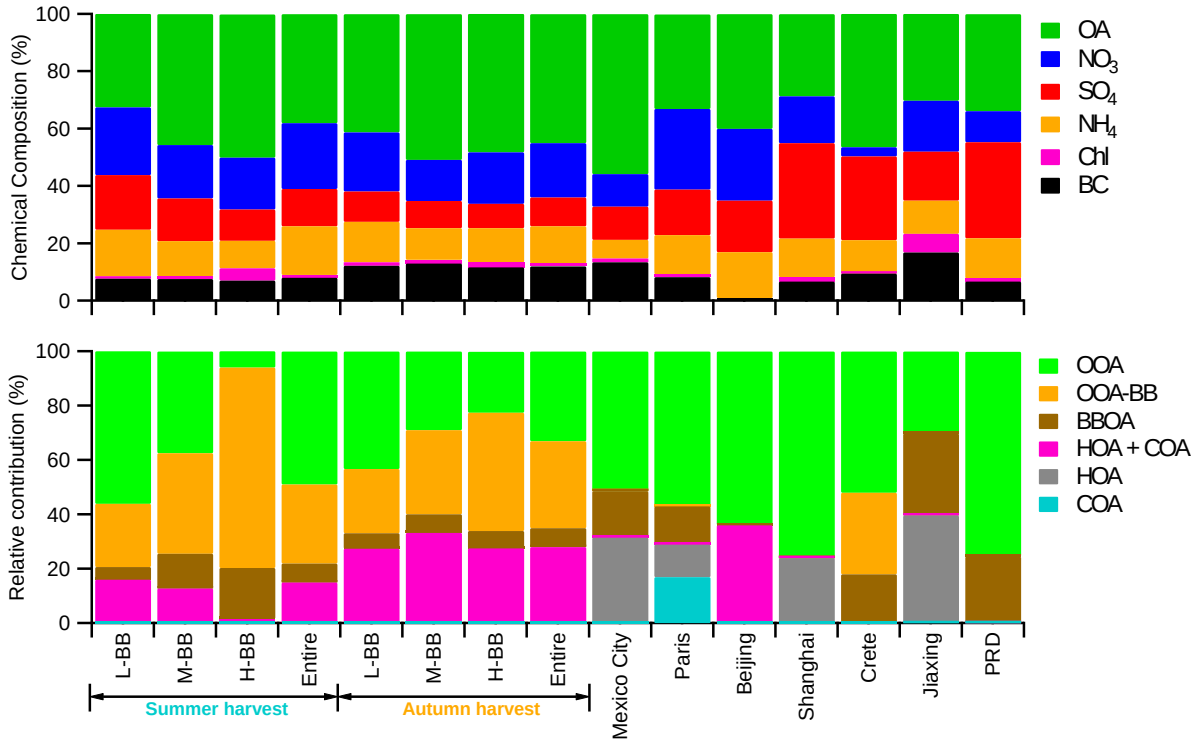

Fig. 7. Average relative contributions of PM_1 species and OA components for low biomass burning period (L-BB), medium biomass burning period (M-BB), and high biomass burning period (H-BB), as well as entire period during the harvest seasons and other sites including mega-cities (Mexico city, Paris, Beijing and Shanghai), suburban area (Jiaxing), remote background site (Crete), and PRD (Pearl River Delta, China). Note that OOA in this plot includes OOA_2-BBOA in Paris.

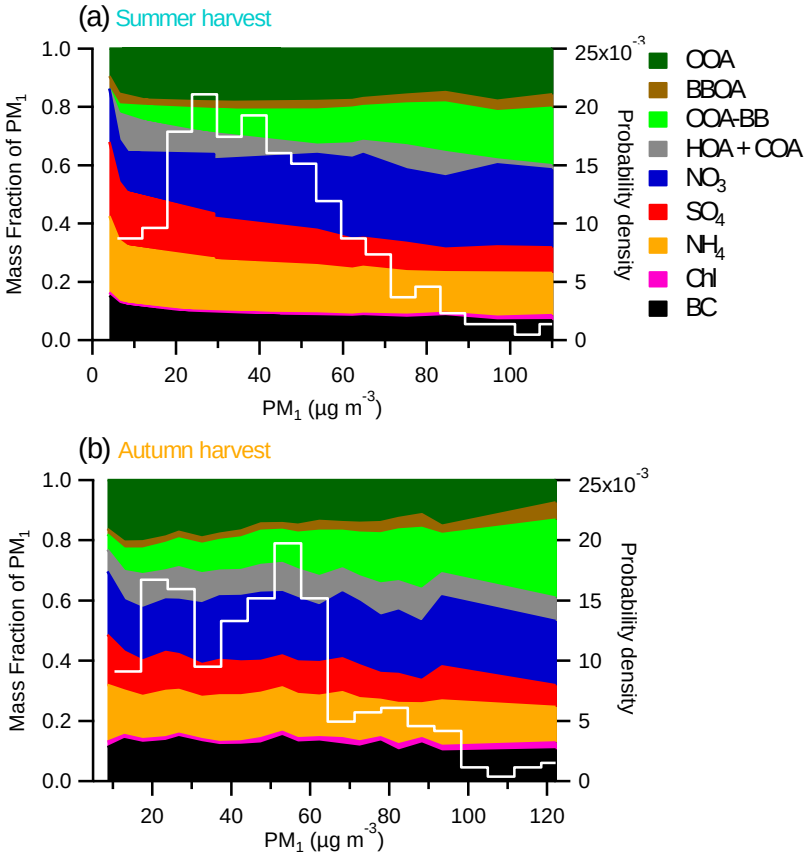

Fig. 8. The mass fractions of PM_1 species and OA components as a function of PM_1 mass loadings (left), and probability density of PM_1 mass loadings (right, with the white lines in the plots) during the summer and autumn harvest respectively.

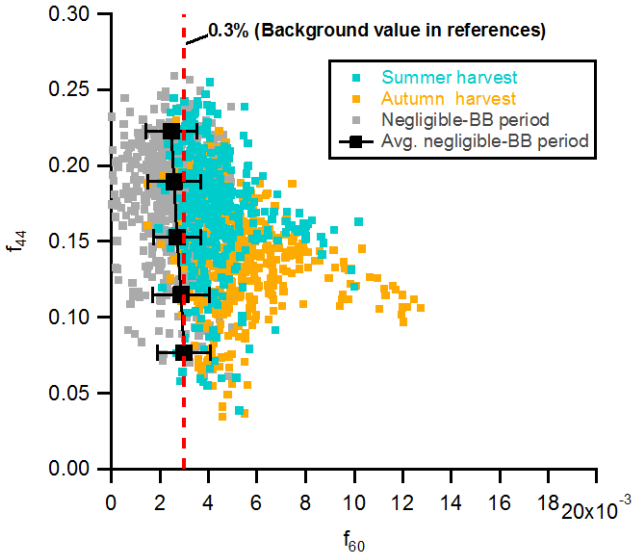

1072

1073 **Fig. 9.** Summary plots showing f_{44} vs. f_{60} for measurements with little or negligible biomass burning
1074 influence. Colored by the summer harvest (blue), autumn harvest (orange), and little or negligible biomass
1075 burning influence period (gray, July 1 to 8, 2013), respectively. Also shown is the average background
1076 level of f_{60} (~0.3%, red dashed line) in other studies from Aiken et al. (2009) and Cubison et al. (2011) for
1077 references.

1078

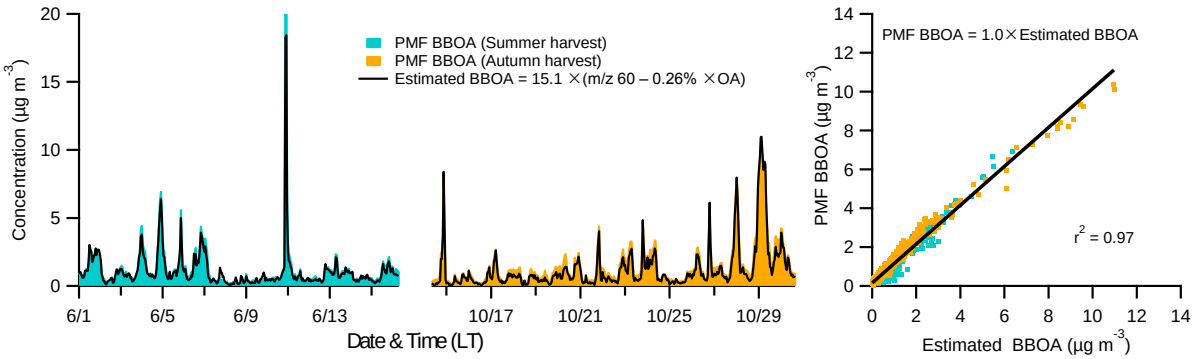

1079

1080 **Fig. 10.** Time series of fresh BBOA identified by PMF (PMF BBOA) and estimated BBOA during the

1081 harvest seasons, as well as correlation plot of estimated BBOA vs. PMF BBOA. Note that the highest

1082 values for case 1 (Fig. 1c) during the summer harvest have been removed for fitting.

1083

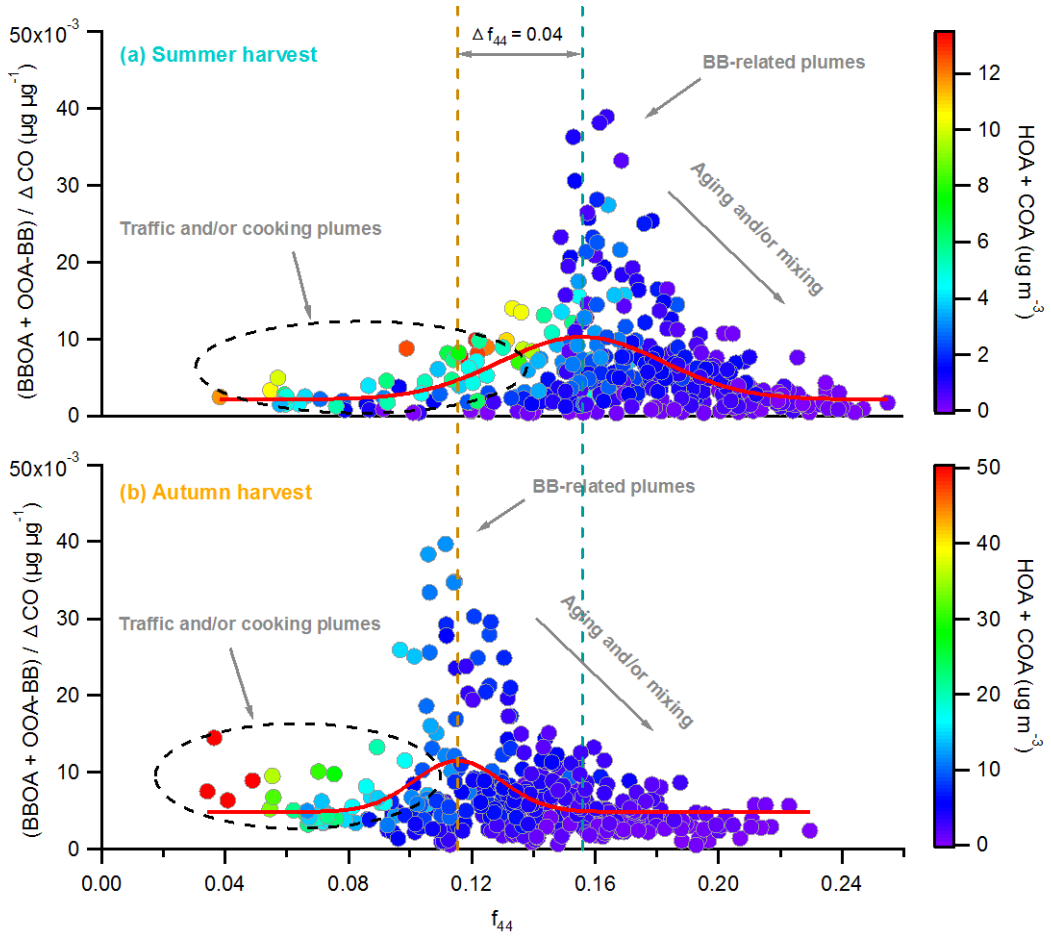

Fig. 11. The (BBOA + OOA-BB) / ΔCO ratio as a function of f_{44} during the summer and autumn harvest. Colored by the HOA + COA mass concentrations, and the red curve lines are the Gaussian fitting for the summer and autumn harvest.

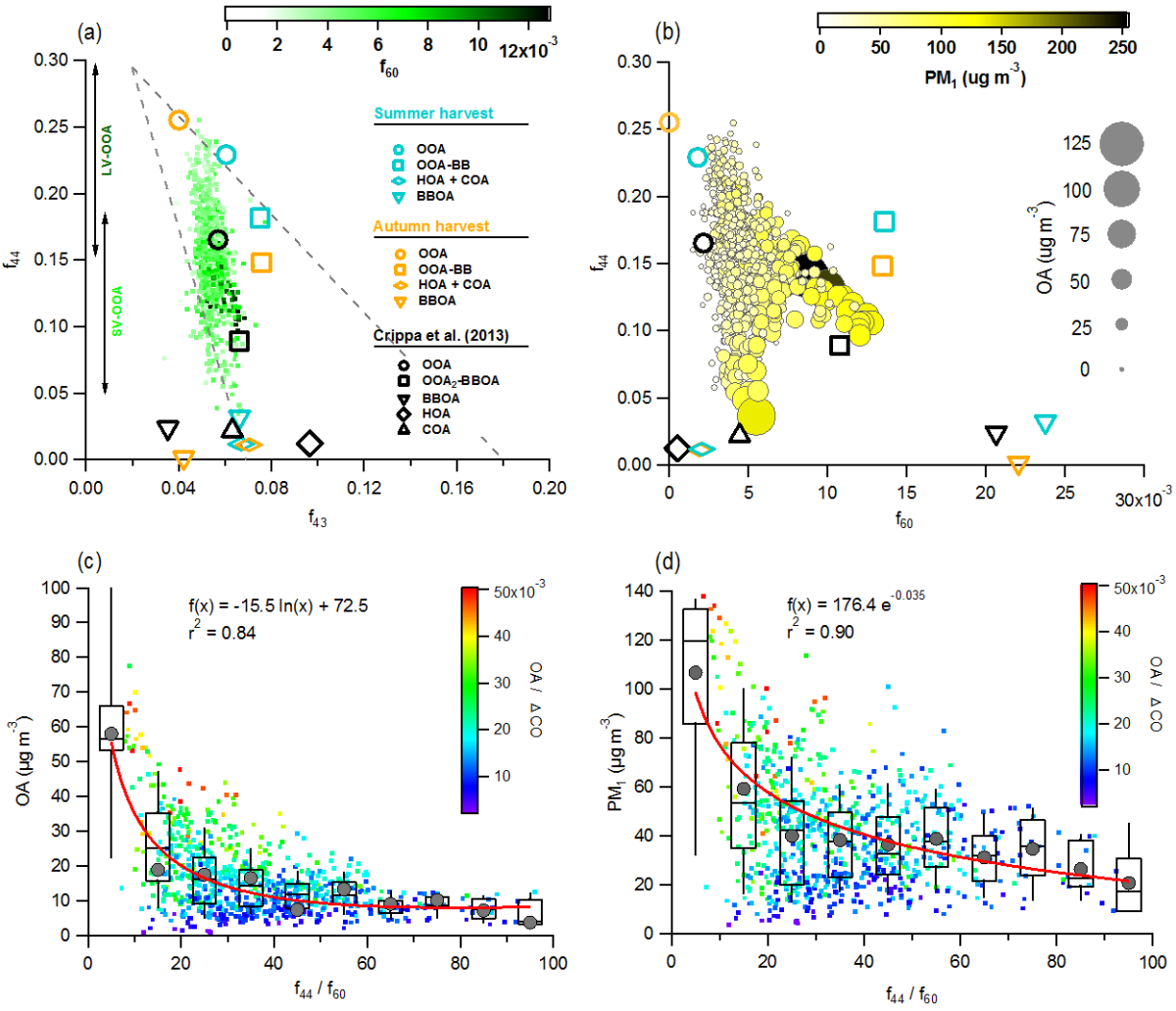

Fig. 12. Summary plots showing **(a)** triangle plot (f_{44} vs. f_{43}), SV-OOA and LV-OOA indicate semi-volatile OOA and low-volatility OOA respectively. The dots are colored by f_{60} as a biomass-burning marker; **(b)** f_{44} as a function of f_{60} (f_{44} vs. f_{60}), colored by the PM_1 mass concentration and sized by the OA loadings; **(c - d)** the total OA and PM_1 mass concentration as a function of the ratio f_{44} / f_{60}, colored by the OA /ΔCO ratio, respectively. Here the mean values (gray points) for curve fitting (c - d) were used.

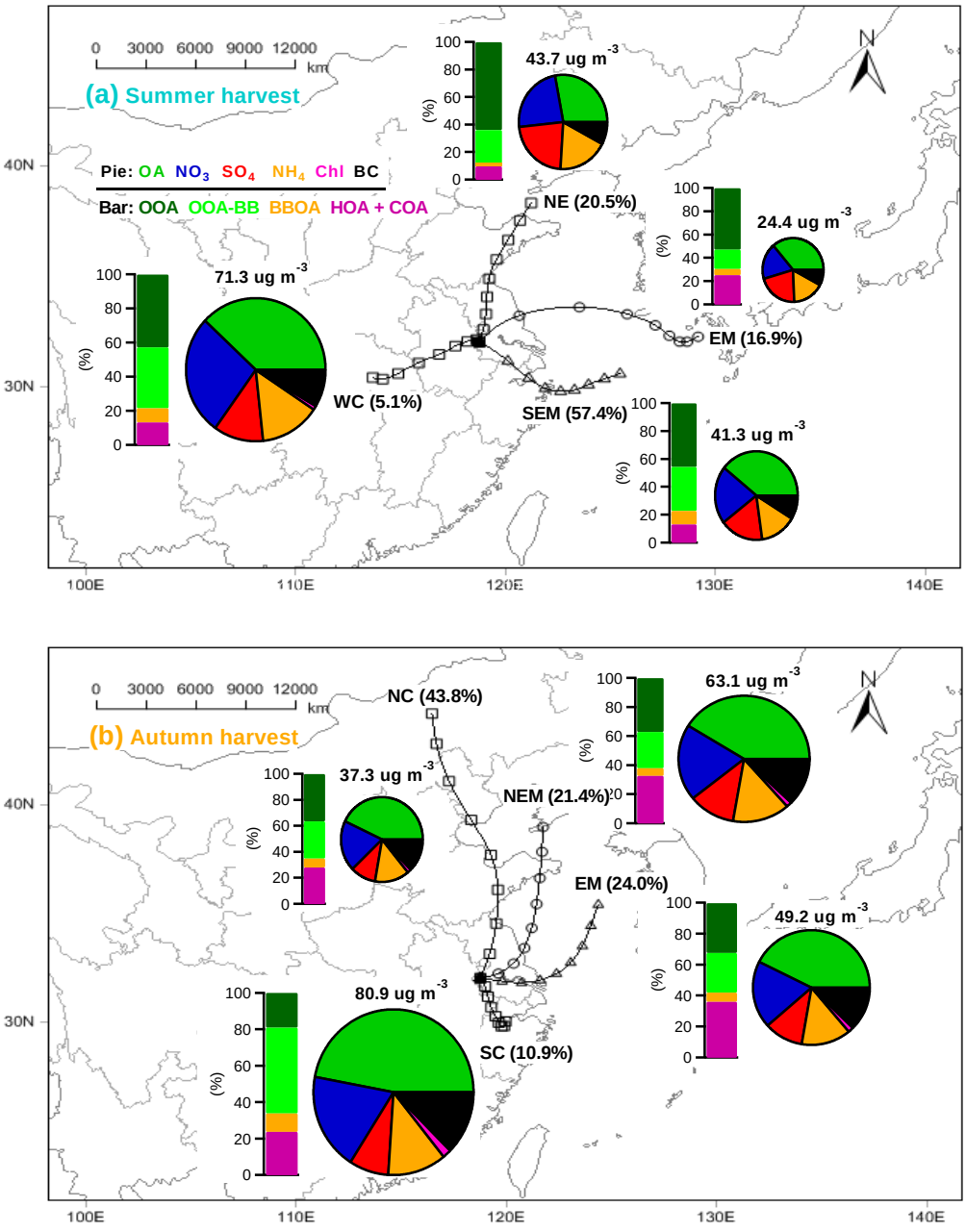

Fig. 13. Average composition of PM_1 (pie charts) and OA factors (bar charts) for each cluster. The four clusters are: **(a)** northeasterly (NE) back-trajectories (BTs), easterly marine (EM) BTs, southeasterly marine (SEM) BTs and westerly continental (WC) during the summer harvest; and **(b)** northerly continental (NC) BTs, northeasterly marine (NEM) BTs, easterly marine (EM) BTs and southerly continental (SC) during the autumn harvest. The markers on the trajectories indicate 6 h interval.